Inorg. Chem. **2006**, *45*, 3325–3343

Silver(I) Coordination Polymers Based on A Nano-Sized Bent Bis(3-acetylenylphenyl-(4-cyanophenyl))oxadiazole Ligand: The Role of Ligand Isomerism and the Templating Effect of Polyatomic Anions and Solvent Intermediates

Yu-Bin Dong,* Hong-Xia Xu, Jian-Ping Ma, and Ru-Qi Huang

College of Chemistry, Chemical Engineering and Materials Science and Shandong Key Lab of Chemical Functional Materials, Shandong Normal University, Jinan 250014, P. R. China.

Received December 19, 2005

One nanosized oxadiazole bridging ligand, bis(3-acetylenylphenyl-(4-cyanophenyl))oxadiazole (**L11**), was designed and synthesized by the reaction of bis(3-iodophenyl)oxadiazole with 4-cyanophenylacetylene via a Sonogashira–Hagihara cross-coupling reaction. Eight Ag(I)–**L11** coordination polymers with one-, two-, or three-dimensional structures have been successfully prepared by the reaction of **L11** with various Ag(I) salts in solution. New coordination polymers were fully characterized by infrared spectroscopy, elemental analysis, and single-crystal X-ray diffraction. All new complexes contain silver heteroatom cluster-connecting nodes, and the **L11** ligand is "doubling up" in the frameworks. In this Ag(I)–**L11** system, the conformation of **L11** is versatile because of the conformational rotation around the central oxadiazole moiety and depends greatly on the counterion and solvent system used in the formation of the complexes. In addition, the luminescence property and host–guest chemistry of some complexes were investigated primarily.

Introduction

Rigid linear organic ligands, such as 4,4′-bipyridine and 4,4′-bibenzonitrile and their various derivatives, are widely used in the construction of coordination polymers and supramolecular complexes by chemists.[1−3] During past decades, the coordination chemistry of rigid linear organic spacers resulted in a number of coordination polymers that exhibit a rich variety of structural motifs with interesting physical and chemical properties. In principle, such kinds of ligands are dominant in generating of linear chain,[4] honeycomblike,[5] adamantoid-like,[6] squarelike,[7] brick-wall-like,[8] and parquetlike[9] structures if they are allowed to

* To whom correspondence should be addressed. E-mail: yubindong@sdnu.edu.cn.

(1) Recent reviews on metal−organic polymers: (a) Yaghi, O. M.; O'Keeffe, M.; Ockwig, N. W.; Chae, H. K.; Eddaoudi, M.; Kim. J. *Nature* **2003**, *423*, 706. (b) Kitagawa, S.; Kitaura, R.; Noro, S.-I.; *Angew. Chem., Int. Ed.* **2004**, *43*, 2334. (c) Zaworotko, M. J.; Moulton, B. *Chem. Rev.* **2001**, *101*, 2619. (d) Eddaoudi, M.; Moler, D. B.; Li, H.; Chen, B.; Reineke, T. M.; Keeffe, M. O.; Yaghi, O. M.; *Acc. Chem. Res.* **2001**, *34*, 319. (e) Constable, E. C. *Prog. Inorg. Chem.* **1994**, *42*, 67. (f) Dunbar, K. R.; Heintz, K. R. *Prog. Inorg. Chem.* **1996**, 283. (g) Whiteford, J. A.; Rachlin, E. M.; Stang, P. J. *Angew. Chem., Int. Ed.* **1996**, *35*, 2524. (h) Hagrman, P. J.; Hagrman, D.; Zubieta, J. *Angew. Chem., Int. Ed.* **1999**, *38*, 2639. (i) Blake, A. J.; Champness, N. R.; Hubberstey, P.; Li, W.-S.; Withersby, M. A.; Schröder, M. *Coord. Chem. Rev.* **1999**, *183*, 117. (j) Batten, S.; Robson, R. *Angew. Chem., Int. Ed.* **1998**, *37*, 1460. (k) Barnett, S. A.; Champness, N. R. *Coord. Chem. Rev.* **2003**, *246*, 145.

(2) (a) Gardner, G. B.; Venkataraman, D.; Moore, J. S.; Lee, S. *Nature* **1995**, *374*, 792. (b) Kiang, Y.-H.; Gardner, G. B.; Lee, S.; Xu, Z. *J. Am. Chem. Soc.* 2**000**, *122*, 6871. (c) Maji, T. K.; Uemura, K.; Chang, H.-C.; Matsuda, R.; Kitagawa, S. *J. Am. Chem. Soc.* **2004**, *126*, 3269. (d) Dybtsev, D. N.; Chun, H.; Yoon, S. H.; Kim, D.; Kim, K. *J. Am. Chem. Soc.* **2004**, *126*, 32. (e) Su, C.-Y.; Goforth, A. M.; Smith, M. D.; Pellechia, P. J.; zur Loye, H.-C. *J. Am. Chem. Soc.* **2004**, *126*, 3576. (f) Zhou, Y.-F.; Jiang, F.-L.; Yuan, D.-Q.; Wu, B.-L.; Wang, R.-H.; Lin, Z.-Z.; Hong, M.-C. *Angew. Chem., Int. Ed.* **2004**, *43*, 5665. (g) Zhang, J.-P.; Zheng, S.-L.; Huang, X.-C.; Chen, X.-M. *Angew. Chem., Int. Ed.* **2003**, *43*, 206. (h) Zhao, B.; Chen, X.-Y.; Cheng, P.; Liao, D.-Z.; Yan, S.-P.; Jiang, Z.-H. *J. Am. Chem. Soc.* **2004**, *126*, 15394. (i) Wu, C.-D.; Lin, W. *Angew. Chem., Int. Ed.* **2005**, *44*, 1958. (j) Kong, L.-Y.; Zhang, Z.-H.; Zhu, H.-F.; Kawaguchi, H.; Okamura, T.-a; Doi, M.; Chu, Q.; Sun, W.-Y.; Ueyama, N. *Angew. Chem., Int. Ed.* **2005**, *44*, 4352. (k) Hanson, K.; Calin, N.; Bugaris, D.; Scancela, M.; Sevov, S. C. *J. Am. Chem. Soc.* **2004**, *126*, 10502. (l) Khlobystov, A. N.; Brett, M. T.; Blake, A. J.; Champness, N. R.; Gill, P. M. W.; O'Neill, D. P.; Teat, S. J.; Wilson, C.; Schröder, M. *J. Am. Chem. Soc.* **2003**, *125*, 6753. (m) Takaoka, K.; Kawano, M.; Tominaga, M.; Fujita, M. *Angew. Chem., Int. Ed.* **2005**, *44*, 2151.

(3) (a) Halper, S. R.; Cohen, S. *Inorg. Chem.* **2005**, *44*, 4139. (b) Burchell, T. J.; Puddephatt, R. J. *Inorg. Chem.* **2005**, *44*, 3718. (c) Chen, W.; Wang, J.-Y.; Chen, C.; Yue, Q.; Yuan, H.-M.; Chen, J.-S.; Wang, S.-N. *Inorg. Chem.* **2003**, *42*, 944. (d) Pan, L.; Huang, X.; Phan, H.-L. N.; Emge, T. J.; Li, J.; Wang, X. *Inorg. Chem.* **2004**, *43*, 6878. (e) Shin, D. M.; Lee, I. S.; Chung, Y. K. *Inorg. Chem.* **2003**, *42*, 8838. (f) Chen, C.-L.; Goforth, A. M.; Smith, M. D.; Su, C.-Y.; zur Loye, H.-C. *Inorg. Chem.* **2005**, *44*, 8762.

10.1021/ic052158w CCC: $33.50
Published on Web 03/14/2006

Chart 1. Some Typical Coordination Motifs Generated from Rigid Linear Organic Ligands

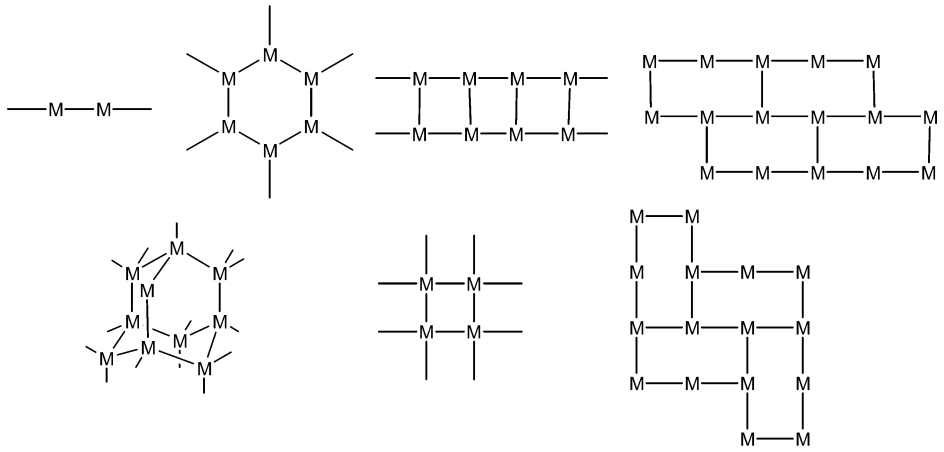

Chart 2. Some Possible Coordination Motifs Generated from Bent Organic Ligands

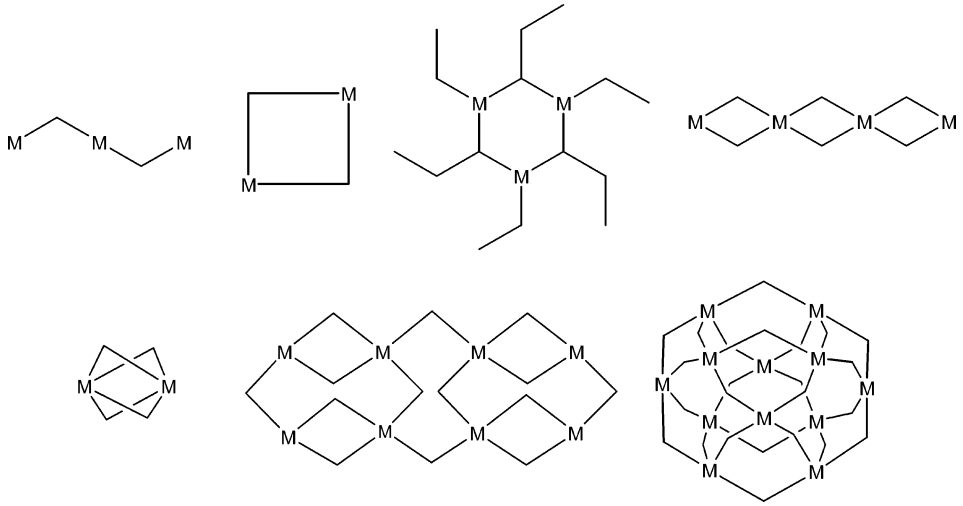

combine with a two-, three-, or four-coordinated metal center (Chart 1). Compared to the well-developed coordination chemistry based on the linear organic ligands, the coordination chemistry related to the bent organic ligands still remains a great challenge. It is obvious that the bent ligands do not propagate the metal-coordination code directly into the metal−organic frameworks, which makes it somewhat more difficult to predict the coordination network topologies. We could image that the bent organic ligands, because of their variational conformation (cis, trans, or any intermediary conformations between them), would offer the possibility for construction of frameworks with novel patterns not easily achievable by linear rigid ligands, such as the helical chain,[10] rhombuslike,[11] distorted-hexagon-like,[12] and many other unprecedented polymeric structures (Chart 2). In addition, bent organic ligands are good candidates for generating molecular polyhedral hollow coordination cages, which are demonstrated in many previous studies.[13]

In the linear ligand's case, the metal center is chosen to be the connecting node to finish the bending in the framework. Unfortunately, the metal coordination mode is often contorted by some ineluctable factors, such as the coordination nature of counterions and the templating of solvent molecules, which affects the formation of the expected polymeric or discrete supramolecular aggregates. In the bent ligand's case, the bending angle could be

(4) Typical Ag(I)−L linear chain examples were summarized in a review by: Blake, A. J.; Champness, N. R.; Hubberstey, P.; Li, W.-S.; Withersby, M. A.; Schröder, M. *Coord. Chem. Rev.* **1999**, *183*, 117.
(5) MacGillivray, L. R.; Subramamian, S.; Zaworotko, M. J. *J. Chem. Soc., Chem. Commun.* **1994**, 1325.
(6) For earlier examples of Ag(I) (4-fold) and Cu(I) (4-fold) diamondoid frameworks based on linear 4, 4′-bipy, see: Carlucci, L.; Ciani, G.; Proserpio, D. M.; Sironi, A. *J. Chem. Soc., Chem. Commun.* **1994**, 2755. An example of an 8-fold interpenetrating diamondoid framework based on tetrahedral Ag(I) and linear 3,3′-dicyanodiphenylacetylene ligand was reported by: Hirsch, K. A.; Wilson, S. R.; Moore, J. S. *Inorg. Chem.* **1997**, *36*, 2960.
(7) Fujita, M.; Kwon, Y. J.; Washizu, S.; Ogura, K. *J. Am. Chem. Soc.* **1994**, *116*, 1151.
(8) (a) Fujita, M.; Kwon, Y. J.; Sasaki, O.; Yamaguchi, K.; Ogura, K. *J. Am. Chem. Soc.* **1995**, *117* (7), 7287. (b) Losier, P.; Zaworotko, M. J. *Angew. Chem., Int. Ed.* **1996**, *35*, 2779.
(9) Dong, Y.-B.; Layland, R. C.; Smith, M. D.; Pschirer, N. G.; Bunz, U. H. F.; zur Loye, H.-C. *Chem. Mater*. **1999**, *11*, 1415.
(10) (a) Shin, D. M.; Lee, I. S.; Chung, Y. K. *Inorg. Chem.* **2003**, *42*, 8838. (b) Reger, D. L.; Semeniuc, R. F.; Rassolov, V.; Smith, M. D. *Inorg. Chem.* **2004**, *43*, 537.
(11) Yaghi, O. M.; Li, H.; Groy, T. L. A. *Inorg. Chem.* **1997**, *36*, 4292.
(12) Abourahma, H.; Moulton, B.; Kravtsov, V.; Zaworotko, M. *J. Am. Chem. Soc.* **2002**, *124*, 9990.
(13) (a) Tominaga, M.; Suzuki, K.; Murase, T.; Fujita, M. *J. Am. Chem. Soc.* **2005**, *127*, 11950. (b) Tominaga, M.; Suzuki, K.; Kawano, M.; Kusukawa, T.; Ozeki, T.; Sakamoto, S.; Yamaguchi, K.; Fujita, M. *Angew. Chem., Int. Ed.* **2004**, *43*, 5621.

Scheme 1. Known 1,3,4-Oxadiazole Bridging Bent Organic Ligands L1−L10

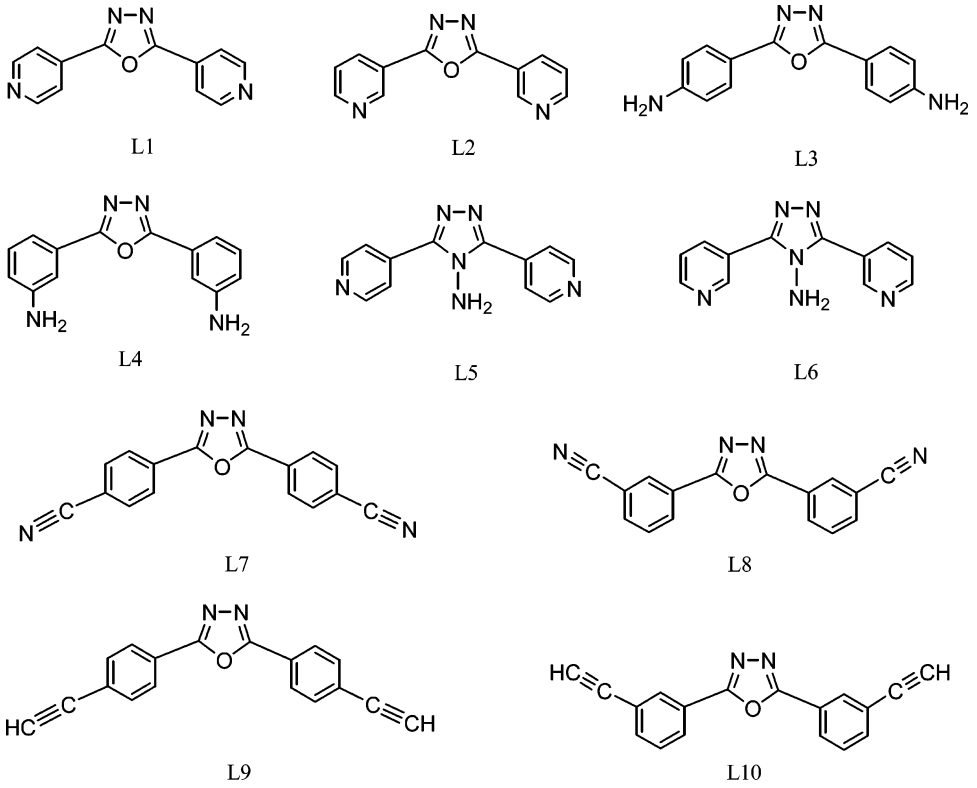

controlled relatively easier and more reliably by the ingenious choice of geometry of the organic bridging moiety. This alternative ligand-directed approach thereby would create opportunities for rational design and construction of specific and desired frameworks more accurately, especially for the hollow molecular-cage-containing complexes.

It is reasonable to say that understanding and insight into the self-assembly process on the basis of bent organic spacers can be improved by carrying out a systemic study using a series of geometrically similar bent-shaped ligands and various inorganic metal cations. Recently, we have designed and synthesized a series of five-membered oxadiazole and triazole heteroatom cyclic rings that are bridging bent organic ligands with pyridyl, cyano, aminophenyl, and acetylenylphenyl groups as the terminal coordination sites (Scheme 1). As a result of the bent geometry of these five-membered heterocyclic bridging ligands and the coordination preferences of transition metals, we have obtained various new coordination polymers, some with open channels and interesting luminescence properties.[14]

As part of our systemic and in-depth investigation of self-assembly on the basis of bent ligands of this type, we herein present the synthesis of a new novel nanometer-sized bent 1, 3, 4-oxadiazole bridging ligand (**L11**) by a Pd-catalyzed coupling reaction and eight new silver coordination polymers, namely, $[Ag_2(\mathbf{L11})SO_3CF_3]_2 \cdot C_6H_6$ (**1**), $[Ag_2(\mathbf{L11})SO_3CF_3]_2 \cdot C_6H_6$ (**2**), $[Ag(\mathbf{L11})]PF_6$ (**3**), $[Ag(\mathbf{L11})SbF_6] \cdot (C_6H_6) \cdot (THF)$ (**4**), $[Ag(\mathbf{L11})]ClO_4 \cdot 2.5(C_6H_6)$ (**5**), $[Ag(\mathbf{L11})]BF_4 \cdot 2.5(C_6H_6)$ (**6**), $[Ag(\mathbf{L11})SbF_6]$·unknown solvate (**7**), and $[Ag(\mathbf{L11})]ClO_4 \cdot (C_7H_8)$ (**8**), generated from **L11** and various silver salts, as shown in Scheme 2.

Experimental Section

Materials and Methods. $AgSO_3CF_3$, $AgClO_4$, $AgBF_4$, and $AgSbF_6$ (Acros) were used as obtained without further purification. Infrared (IR) samples were prepared as KBr pellets, and spectra were obtained in the 400−4000 cm^{-1} range using a Perkin-Elmer 1600 FTIR spectrometer. Elemental analyses were performed on a Perkin-Elmer Model 2400 analyzer. ^1H NMR data were collected using an AM-300 spectrometer. Chemical shifts are reported in δ relative to TMS. All fluorescence measurements were carried out on a Cary Eclipse Spectrofluorimeter (Varian, Australia) equipped with a xenon lamp and quartz carrier at room temperature. Thermogravimetric analyses were carried out using a TA Instrument SDT 2960 simultaneous DTA−TGA under flowing nitrogen at a heating rate of 10 °C/min. XRD patterns were obtained on a D8

(14) (a) Dong, Y.-B.; Ma, J.-P.; Smith, M. D.; Huang, R.-Q.; Tang, B.; Chen, D.; zur Loye, H.-C. *Solid State Sci.* **2002**, *4*, 1313. (b) Dong, Y.-B.; Ma, J.-P.; Huang, R.-Q.; Smith, M. D.; zur Loye, H.-C. *Inorg. Chem.* **2003**, *42*, 294. (c) Dong, Y.-B.; Ma, J.-P.; Smith, M. D.; Huang, R.-Q.; Tang, B.; Guo, D.-S.; Wang, J.-S.; zur Loye, H.-C. *Solid State Sci.* **2003**, *5*, 601. (d) Dong, Y.-B.; Ma, J.-P.; Smith, M. D.; Huang, R.-Q.; Wang, J.-S.; zur Loye, H.-C. *Solid State Sci.* **2003**, *5*, 1177. (e) Dong, Y.-B.; Cheng, J.-Y.; Wang, H.-Y.; Huang, R.-Q.; Tang, B.; Smith, M. D.; zur Loye, H.-C. *Chem. Mater.* **2003**, *15*, 2593. (f) Dong, Y.-B.; Ma, J.-P.; Huang, R.-Q.; Liang, F.-Z.; Smith, M. D. *J. Chem. Soc., Dalton Trans.* **2003**, *9*, 1472. (g) Dong, Y.-B.; Cheng, J.-Y.; Huang, R.-Q.; Tang, B.; Smith, M. D.; zur Loye, H.-C. *Inorg. Chem.* **2003**, *42*, 5699. (h) Cheng, J.-Y.; Dong, Y.-B.; Ma, J.-P.; Huang, R.-Q.; Smith, M. D. I*norg. Chem. Commun.* **2005**, *8*, 6. (i) Dong, Y.-B.; Cheng, J.-Y.; Huang, R.-Q.; Smith, M. D. *Inorg. Chim. Acta* **2005**, *358*, 891. (j) Dong, Y.-B.; Cheng, J.-Y.; Ma, J.-P.; Huang, R.-Q.; Smith, M. D. *Cryst. Growth Des.* **2005**, *5*, 585. (k) Dong, Y.-B.; Wang, H.-Y.; Ma, J.-P.; Huang, R.-Q.; Smith, M. D. *Cryst. Growth Des.* **2005**, *5*, 789. (l) Wang, P.; Dong, Y.-B.; Ma, J.-P.; Huang, R.-Q.; Smith, M. D. *Inorg. Chem. Commun.* **2005**, *8*, 596. (m) Dong, Y.-B.; Wang, H.-Y.; Ma, J.-P.; Shen, D.-Z.; Huang, R.-Q. *Inorg. Chem.* **2005**, *44*, 4679. (n) Dong, Y.-B.; Zhang, Q.; Wang, L.; Ma, J.-P.; Huang, R.-Q.; Shen, D.-Z.; Chen, D.-Z. *Inorg. Chem.* **2005**, *44*, 6591. (o) Ma, J.-P.; Dong, Y.-B.; Huang, R.-Q.; Smith, M. D.; Su, C.-Y. *Inorg. Chem.* **2005**, *44*, 6143.

Scheme 2. Synthesis of New Ligand **L11** and Compounds **1**−**8**

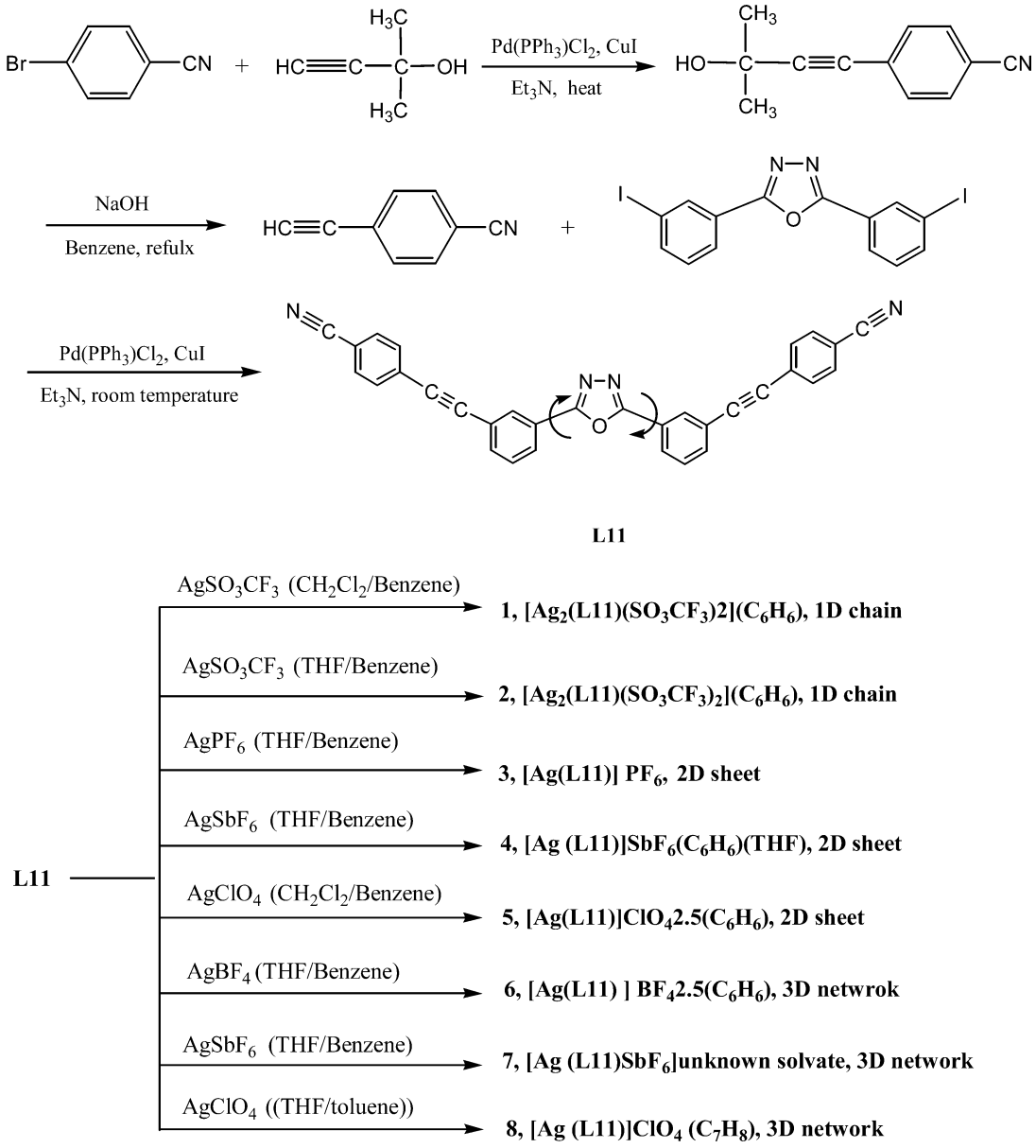

ADVANCE X-ray powder diffractometer (XRD) with Cu Ka radiation (λ = 1.5405 Å).

Caution! *Two of the crystallization procedures involve $AgClO_4$, which is a strong oxidizer.*

Preparation of L11. 4-Cyanophenylacetylene (2.0 mmol), bis-(3-iodophenyl)oxadiazole (1.0 mmol), $(Ph_3P)PdCl_2$ (0.044 mmol), and CuI (0.132 mmol) were placed into a flame-dried Schlenk flask. Next, Et_3N (30 mL) and THF (10 mL) were added to the flask. The mixture was stirred at room temperature for 24 h. After removal of the solvent under vacuum, the residue was purified on silica gel by a column using CH_2Cl_2 as the eluent to afford **L11** as a colorless crystalline solid (Yield, 90%). IR (KBr pellet, cm^{-1}): 2224 (s), 1602 (s), 1541 (ms), 1501 (ms), 1463 (ms), 1404 (w), 1317 (w), 1257 (w), 1136 (w), 1086 (w), 973 (w), 903 (w), 880 (w), 839 (s), 805 (m), 734 (m), 683 (m), 556 (m). ^1H NMR (300 MHz, $CDCl_3$, 25 °C, TMS, ppm): 8.33 (s, 2H, $-C_6H_4$), 8.20−8.17 (d, 2H, $-C_6H_4$), 7.75−7.56 (m, 12H, $-C_6H_4$). Anal. Calcd. for $C_{32}H_{16}N_4O$: C, 81.36; H, 3.39; N, 11.86. Found: C, 81.15; H, 3.28; N, 11.47. Mp: 264−266 °C.

Preparation of $[Ag_2(L11)SO_3CF_3]_2 \cdot C_6H_6$ (1). A solution of $AgSO_3CF_3$ (5.44 mg, 0.021 mmol) in benzene (10 mL) was layered onto a solution of **L11** (10.0 mg, 0.021 mmol) in CH_2Cl_2 (10 mL). The solutions were left for about one week at room temperature, and colorless crystals were obtained. Yield, 55%. IR (KBr, cm^{-1}): 2225 (m), 1626 (m), 1603 (m), 1542 (m), 1502 (w), 1467 (w), 1404 (m), 1251 (vs), 1171 (s), 1104 (w), 1035 (s), 900 (w), 880 (w), 839 (m), 803 (w), 763 (w), 735 (m), 683 (m), 645 (s), 578 (w), 554 (m), 519 (m). ^1H NMR (300 MHz, DMSO, 25 °C, TMS, ppm): 8.40 (s, 2H, $-C_6H_4$), 8.27−8.25 (d, 2H, $-C_6H_4$), 7.95−7.81 (m, 10H, $-C_6H_4$), 7.76−7.71 (t, 2H, $-C_6H_4$), 7.37 (s, C_6H_6). Anal. Calcd. for $C_{40}H_{22}Ag_2F_6N_4O_7S_2$: C, 45.09; H, 2.07; N, 5.26. Found: C, 45.00; H, 2.23; N, 5.33.

Preparation of $[Ag_2(L11)SO_3CF_3]_2 \cdot C_6H_6$ (2). A solution of $AgSO_3CF_3$ (5.44 mg, 0.021 mmol) in benzene (10 mL) was layered onto a solution of **L11** (10.0 mg, 0.021 mmol) in THF (10 mL). The solutions were left for about one week at room temperature, and colorless crystals were obtained. Yield, 50%. IR (KBr pellet, cm^{-1}): 2226 (m), 1602 (m), 1542 (m), 1502 (m), 1465 (m), 1404

(w), 1258 (vs), 1174 (s), 1084 (w), 1034 (s), 880 (w), 839 (m), 804 (w), 763 (w), 736 (w), 683 (m), 645 (s), 577 (w), 555 (m), 518 (m). ^{1}H NMR (300 MHz, DMSO, 25 °C, TMS, ppm): 8.39 (s, 2H, $-C_6H_4$), 8.27−8.25 (d, 2H, $-C_6H_4$), 7.95−7.87 (m, 6H, $-C_6H_4$), 7.84−7.81 (d, 4H, $-C_6H_4$), 7.76−7.71 (t, 2H, $-C_6H_4$), 7.36 (s, C_6H_6). Anal. Calcd. for $C_{40}H_{22}Ag_2F_6N_4O_7S_2$: C, 45.09; H, 2.07; N, 5.26. Found: C, 45.01; H, 2.00; N, 5.08.

Preparation of [Ag(L11)]PF_6 (3). A solution of $AgPF_6$ (5.31 mg, 0.021 mmol) in benzene (10 mL) was layered onto a solution of **L11** (10.0 mg, 0.021 mmol) in THF (10 mL). The solutions were left for about one week at room temperature, and colorless crystals were obtained. Yield, 49%. IR (KBr pellet cm^{-1}): 2226 (m), 1649 (w), 1600 (m), 1543 (m), 1502 (m), 1458 (m), 1402 (s), 1318 (w), 1267 (w), 1179 (w), 1139 (w), 1089 (w), 835 (vs), 741 (m), 683 (s), 555 (s). ^{1}H NMR (300 MHz, DMSO, 25 °C, TMS, ppm): 8.40 (s, 2H, $-C_6H_4$), 8.28−8.25 (d, 2H, $-C_6H_4$), 7.96−7.93 (d, 4H, $-C_6H_4$), 7.90−7.88 (d, 2H, $-C_6H_4$), 7.84−7.81 (d, 4H, $-C_6H_4$), 7.76−7.71 (t, 2H, $-C_6H_4$). Anal. Calcd. for $C_{32}H_{16}AgF_6N_4OP$: C, 52.94; H, 2.21; N, 7.72. Found: C, 52.89; H, 2.16; N, 7.69.

Preparation of [Ag(L11)SbF_6]·(C_6H_6)·(THF) (4) and [Ag(L11)SbF_6]·unknown solvate (7). A solution of $AgSbF_6$ (7.26 mg, 0.021 mmol) in benzene (10 mL) was layered onto a solution of **L11** (10.0 mg, 0.021 mmol) in THF (10 mL). The solutions were left for about one week at room temperature, and colorless blocklike crystals (**4** and **7**) were obtained. The combined crystal yield was 8.57 mg (50%). IR (KBr pellet, cm^{-1}): 2249 (w), 2226 (m), 1828 (w), 1635 (w), 1602 (s), 1541 (m), 1501 (m), 1466 (m), 1449 (m), 1402 (s), 1318 (w), 1260 (w), 1180 (w), 1136 (w), 1106 (w), 1088 (w), 1060 (w), 922 (w), 903 (w), 881 (w), 842 (s), 817 (w), 805 (m), 735 (m), 684 (vs), 659 (vs), 556 (s). ^{1}H NMR (300 MHz, DMSO, 25 °C, TMS, ppm): 8.40 (s, 2H, $-C_6H_4$), 8.28−8.25 (d, 2H, $-C_6H_4$), 7.96−7.88 (m, 6H, $-C_6H_4$), 7.84−7.81 (d, 4H, $-C_6H_4$), 7.76−7.71 (t, 2H, $-C_6H_4$), 7.36 (s, C_6H_6), 3.60 (s, C_4H_8O), 1.90 (s, C_4H_8O). Anal. Calcd. for $C_{42}H_{30}AgF_6N_4O_2Sb$: C, 52.15; H, 3.10; N, 5.80. Found: C, 51.09; H, 2.91; N, 5.82.

Preparation of [Ag(L11)]ClO_4·2.5(C_6H_6) (5). A solution of $AgClO_4$ (4.39 mg, 0.021 mmol) in benzene (10 mL) was layered onto a solution of **L11** (10.0 mg, 0.021 mmol) in CH_2Cl_2 (10 mL). The solutions were left for about one week at room temperature, and colorless crystals were obtained. Yield, 51%. IR (KBr pellet, cm^{-1}): 2224 (m), 1600 s), 1544 s), 1501 (s), 1466 (m), 1402 (vs), 1321 (w), 1256 (w), 1177 (w), 1090 (vs), 910 (w), 878 (m), 841 (m), 804 (w), 738 (m), 682 (m), 621 (s), 555 (m). ^{1}H NMR (300 MHz, DMSO, 25 °C, TMS, ppm): 8.40 (s, 2H, $-C_6H_4$), 8.28−8.25 (d, 2H, $-C_6H_4$), 7.96−7.81 (m, 10H, $-C_6H_4$), 7.76−7.71 (t, 2H, $-C_6H_4$), 7.37 (s, C_6H_6). Anal. Calcd. for $C_{47}H_{31}AgClN_4O_5$: C, 64.45; H, 3.54; N, 6.40. Found: C, 64.29; H, 3.50; N, 6.27.

Preparation of [Ag(L11)]BF_4·2.5(C_6H_6) (6). A solution of $AgBF_4$ (4.11 mg, 0.021 mmol) in benzene (10 mL) was layered onto a solution of L1 (10.0 mg, 0.021 mmol) in THF (10 mL). The solutions were left for about one week at room temperature, and colorless crystals were obtained. Yield, 51%. ^{1}H NMR (300 MHz, DMSO, 25 °C, TMS, ppm): 8.38 (s, 2H, $-C_6H_4$), 8.26−8.23 (d, 2H, $-C_6H_4$), 7.94−7.80 (m, 10H, $-C_6H_4$), 7.74−7.72 (t, 2H, $-C_6H_4$), 7.35 (s, C_6H_6). IR (KBr, cm^{-1}): 3089 (w), 3035 (w), 2260 (w), 2225 (m), 1961 (w), 1824 (w), 1645 (w), 1601 (s), 1542 (s), 1501 (m), 1470 (m), 1405 (w), 1319 (w), 1271 (w), 1082 (vs), 1032 (vs), 902 (w), 881 (w), 838 (s), 805 (m), 735 (m), 678 (vs), 554 (m), 519 (w), 465 (w). Anal. Calcd. for $C_{47}H_{31}AgBF_4N_4O$: C, 65.40; H, 3.59; N, 6.49. Found: C, 65.29; H, 3.51; N, 6.42.

Preparation of [Ag(L11)]ClO_4·(C_7H_8) (8). A solution of $AgClO_4$ (4.39 mg, 0.021 mmol) in benzene (10 mL) was layered onto a solution of **L11** (10.0 mg, 0.021 mmol) in toluene (10 mL). The solutions were left for about one week at room temperature, and colorless crystals were obtained. Yield, 50%. IR (KBr pellet, cm^{-1}): 3071 (w), 2252 (m), 2224 (m), 1639 (w), 1600 (s), 1549 (m), 1502 (m), 1483 (w), 1408 (m), 1322 (w), 1256 (w), 1181 (w), 1087 (vs), 996 (m), 874 (w), 841 (m), 805 (w), 738 (m), 681 (m), 621 (m), 553 (m). ^{1}HNMR (300 MHz, DMSO, 25 °C, TMS, ppm): 8.40 (s, 2H, $-C_6H_4$), 8.28−8.25 (d, 2H, $-C_6H_4$), 7.96−7.82 (m, 10H, $-C_6H_4$), 7.76−7.71 (t, 2H, $-C_6H_4$), 7.25−7.18 (m, C_6H_5), 2.30 (s, $-CH_3$). Anal. Calcd. for $C_{39}H_{24}AgClN_4O_5$: C, 60.63; H, 3.11; N, 7.25. Found: C, 60.40; H, 3.02; N, 7.13.

Single-Crystal Structure Determination. Suitable single crystals of **L11** and **1**−**8** were selected and mounted in air onto thin glass fibers. X-ray intensity data were measured at 293 K on a Bruker SMART APEX CCD-based diffractometer (Mo Kα radiation, $\lambda = 0.71073$ Å). The raw frame data for **L11** and **1**−**8** were integrated into SHELX format reflection files and corrected for Lorentz and polarization effects using SAINT.[15] Corrections for incident and diffracted beam absorption effects were applied using SADABS.[15] None of the crystals showed evidence of crystal decay during data collection. All structures were solved by a combination of direct methods and difference Fourier syntheses and refined against F^2 by the full-matrix least-squares technique. Crystal data, data collection parameters, and refinement statistics for **L11** and **1**−**8** are listed in Tables 1 and 2. Relevant interatomic bond distances and bond angles for **1**−**8** are given in Tables 3−10, respectively.

Results and Discussion

Ligand Synthesis. One of the important issues in determining the dimensions of porous frameworks is the scale of the organic ligands.[16] In principle, the longer the spacers used, the larger pore dimensions would be obtained. To achieve frameworks with larger-sized channels, we designed and synthesized ligand **L11**, which has a bis(4-cyanophenyl)-substituted bent 2,5-bis(3-ethynylphenyl)-1,3,4-oxadiazole backbone involving two symmetric acetylene spacers. This large-length-scale ligand **L11** was synthesized by the reaction of bis(3-iodophenyl)oxadiazole with 4-cyanophenylacetylene via a classical Sonogashira−Hagihara cross-coupling reaction (Scheme 2).[17] When bis(3-iodophenyl)oxadiazole in a Et_3N/THF mixed-solvent system under an inert atmosphere at room temperature was treated with 4-cyanophenylacetylene in a 1:2 molar ratio, we obtained **L11** as a white crystalline solid in 90% yield. The results herein demonstrated that a 1, 3, 4-oxadiazole heterocyclic ring is stable under our experimental conditions. **L11** is soluble in common polar organic solvents such as CH_2Cl_2, $CHCl_3$, CH_3CN, and THF, which potentially facilitates the solution reaction between the ligand and inorganic metal salts. To further confirm the structure of **L11**, we performed single-crystal X-ray diffraction on it. As shown in Figure 1, the ligand is bent, which

(15) *SADABS* and *SAINT*; Bruker Analytical X-ray Systems, Inc.: Madison, WI, 1998.
(16) (a) Pschirer, N. G.; Ciurtin, D. M.; Smith, M. D.; Bunz, U. H. F.; zur Loye, H.-C. *Angew. Chem., Int. Ed.* 2002, *41*, 583. (b) Biradha, K.; Fujita, M. *Chem. Commun*. **2001**, 15. (c) Stang, P.-J.; Cao, D. H.; Saito, S.; Arif, A. M. *J. Am. Chem. Soc.* **1995**, *117*, 6273. (d) Stang, P. J.; Olenyuk, B. *Acc. Chem. Res.* **1977**, *30*, 502.
(17) Sonogashira, K.; Tohda, Y.; Hagihara, N. *Tetrahedron Lett*. **1975**, 4467.

Table 1. Crystallographic Data for **L11** and **1**−**3**

	$C_{32}H_{16}N_4O$ **L11**	$C_{40}H_{22}Ag_2F_6N_4O_7S_2$ **1**	$C_{40}H_{22}Ag_2F_6N_4O_7S_2$ **2**	$C_{32}H_{16}AgF_6N_4OP$ **3**	$C_{42}H_{30}AgF_6N_4O_2Sb$ **4**
fw	472.49	1064.48	1064.48	725.33	966.32
cryst syst	monoclinic	triclinic	triclinic	triclinic	triclinic
a (Å)	18.088(4)	10.181(2)	10.8840(16)	10.7276(14)	10.7908(7)
b (Å)	5.9662(14)	12.826(3)	13.0047(19)	12.2969(16)	12.5144(8)
c (Å)	23.981(5)	17.657(4)	16.524(3)	16.825(2)	16.8103(11)
α (deg)	90	94.202(3)	104.084(2)	111.228(2)	111.4810(10)
β (deg)	110.751(3)	97.789(3)	94.263(2)	105.754(2)	105.9500(10)
γ (deg)	90	110.376(3)	104.432(2)	16.825(2)	93.8490(10)
V (Å^3)	2420.2(10)	2123.2(8)	2174.2(6)	1957.6(4)	1995.0(2)
space group	*C*2/*c*	P$\bar{1}$	P$\bar{1}$	P$\bar{1}$	P1
Z	4	2	2	2	2
ρ_{calcd} (g/cm^3)	1.297	1.665	1.626	1.231	1.609
μ (Mo Kα; mm^{-1})	0.081	1.100	1.074	0.610	1.236
T (K)	293(2)	293(2)	293(2)	293(2)	293(2)
no. of observations ($I > 3\sigma$)	4244	8092	7908	6702	8494
final *R* indices[a] [$I > 2\sigma(I)$] (*R*; R_w)	0.0458; 0.1089	0.0570; 0.1332	0.0511; 0.1330	0.0817; 0.2159	0.0429; 0.0998

[a] $R1 = \sum||F_o| - |F_c||/\sum|F_o|$. $wR2 = \{\sum[w(F_o^2 - F_c^2)^2]/\sum[w(F_o^2)^2]\}^{1/2}$.

Table 2. Crystallographic Data for **5**−**8**

	$C_{47}H_{31}AgClN_4O_5$ **5**	$C_{47}H_{31}AgBF_4N_4O$ **6**	$C_{32}H_{16}AgF_6N_4OSb$ **7**	$C_{39}H_{24}AgClN_4O_5$ **8**
fw	875.08	862.44	816.11	771.94
cryst syst	triclinic	orthorhombic	orthorhombic	monoclinic
a (Å)	10.2064(19)	19.008(3)	23.124(2)	19.328(4)
b (Å)	12.622(2)	24.794(4)	37.368(5)	23.253(5)
c (Å)	17.865(3)	34.955(6)	19.180(2)	19.734(4)
α (deg)	72.553(3)	90	90	90
β (deg)	82.615(3)	90	90	118.073(4)
γ (deg)	71.626(3)	90	90	90
V (Å^3)	2082.1(7)	16474(5)	16574(4)	4244.0(9)
space group	P$\bar{1}$	*Fddd*	*Fdd*2	*C*2/*c*
Z	2	2	16	8
ρ_{calcd} (g/cm^3)	1.369	1.391	1.308	1.310
μ (Mo Kα; mm^{-1})	0.599	0.548	1.176	0.628
T (K)	293(2)	293(2)	293(2)	293(2)
no. of observations ($I > 3\sigma$)	7624	3830	7238	6839
final *R* indices[a] [$I > 2\sigma(I)$] (*R*; R_w)	0.0564; 0.1163	0.0593; 0.1355	0.0634; 0.1442	0.0993; 0.2138

[a] $R1 = \sum||F_o| - |F_c||/\sum|F_o|$. $wR2 = \{\sum[w(F_o^2 - F_c^2)^2]/\sum[w(F_o^2)^2]\}^{1/2}$.

Table 3. Interatomic Distances (Å) and Bond Angles (deg) for **1**[a]

Ag(1)−N(4)#1	2.130(5)	Ag(1)−N(1)	2.263(4)
Ag(1)−O(5)	2.427(5)	Ag(1)−O(2)	2.571(5)
Ag(2)−N(3)#2	2.144(5)	Ag(2)−N(2)	2.276(4)
Ag(2)−O(2)	2.414(4)	Ag(2)−O(5)	2.596(6)
N(4)#1−Ag(1)−N(1)	146.42(18)	N(4)#1−Ag(1)−O(5)	120.6(2)
N(1)−Ag(1)−O(5)	89.58(18)	N(4)#1−Ag(1)−O(2)	113.94(19)
N(1)−Ag(1)−O(2)	83.86(14)	O(5)−Ag(1)−O(2)	79.54(18)
N(3)#2−Ag(2)−N(2)	148.2(2)	N(3)#2−Ag(2)−O(2)	123.0(2)
N(2)−Ag(2)−O(2)	86.47(14)	N(3)#2−Ag(2)−O(5)	112.5(2)
N(2)−Ag(2)−O(5)	82.41(17)	O(2)−Ag(2)−O(5)	79.28(18)

[a] Symmetry transformations used to generate equivalent atoms: #1 $-x + 1, -y + 2, -z$; #2 $-x + 3, -y + 1, -z + 1$.

Table 4. Interatomic Distances (Å) and Bond Angles (deg) for **2**[a]

Ag(1)−N(3)#1	2.136(4)	Ag(1)−N(2)	2.299(3)
Ag(1)−O(5)	2.425(5)	Ag(1)−O(2)	2.554(5)
Ag(2)−N(4)#2	2.141(4)	Ag(2)−N(1)	2.307(3)
Ag(2)−O(2)	2.452(4)	Ag(2)−O(5)	2.452(5)
N(3)#1−Ag(1)−N(2)	139.35(17)	N(3)#1−Ag(1)−O(5)	125.72(19)
N(2)−Ag(1)−O(5)	88.42(16)	N(3)#1−Ag(1)−O(2)	121.33(17)
N(2)−Ag(1)−O(2)	84.60(13)	O(5)−Ag(1)−O(2)	76.33(16)
N(4)#2−Ag(2)−N(1)	137.47(16)	N(4)#2−Ag(2)−O(2)	128.59(16)
N(1)−Ag(2)−O(2)	85.96(12)	N(4)#2−Ag(2)−O(5)	120.10(18)
N(1)−Ag(2)−O(5)	87.55(16)	O(2)−Ag(2)−O(5)	77.77(17)

[a] Symmetry transformations used to generate equivalent atoms: #1 $-x, -y + 1, -z$; #2 $-x + 2, -y, -z + 1$.

Table 5. Interatomic Distances (Å) and Bond Angles (deg) for **3**[a]

Ag(1)−N(2)#1	2.282(5)	Ag(1)−N(1)	2.285(5)
Ag(1)−N(3)#2	2.364(7)	Ag(1)−N(4)#3	2.418(8)
N(2)#1−Ag(1)−N(1)	118.64(17)	N(2)#1−Ag(1)−N(3)#2	109.5(2)
N(1)−Ag(1)−N(3)#2	115.2(2)	N(2)#1−Ag(1)−N(4)#3	113.0(2)
N(1)−Ag(1)−N(4)#3	109.4(3)	N(3)#2−Ag(1)−N(4)#3	86.7(3)

[a] Symmetry transformations used to generate equivalent atoms: #1 $-x + 2, -y + 1, -z + 1$; #2 $-x + 2, -y + 1, -z$; #3 $x, y - 1, z - 1$; #4 $x, y + 1, z + 1$.

is similar to the shape of known organic spacers L1−L10. The separation between two terminal N-donors is ∼24 Å, which is remarkably longer than those corresponding distances found in L1−L10. It is noteworthy that two ethynylbenzonitrilephenyl moieties are connected via two *exo*-oxadiazole carbon−carbon single bonds at the 2,5-positions to create the bent spacer, in which two long arms can rotate freely around the single carbon−carbon bonds. Thus, **L11** is flexible and very useful in construction of elaborate metal−organic complexes. Scheme 3 presents three possible typical conformations of **L11**. The ab initio Mulliken population analysis of **L11** shows that the energies of three possible typical conformations of **L11** in either gas or benzene solution are almost identical;[18] thus, these three conformations (I, II, and III) could be concomitant in gas or benzene solution. Therefore, the conformation of **L11** adopted in the

Table 6. Interatomic Distances (Å) and Bond Angles (deg) for **4**[a]

Ag(1)−N(4)#1	2.257(9)	Ag(1)−N(6)	2.278(6)
Ag(1)−N(2)	2.327(7)	Ag(1)−N(8)#2	2.499(10)
Ag(2)−N(5)	2.282(7)	Ag(2)−N(3)#3	2.282(9)
Ag(2)−N(1)	2.328(7)	Ag(2)−N(7)#4	2.473(9)
N(4)#1−Ag(1)−N(6)	119.6(3)	N(4)#1−Ag(1)−N(2)	112.2(3)
N(6)−Ag(1)−N(2)	119.0(2)	N(4)#1−Ag(1)−N(8)#2	86.6(3)
N(6)−Ag(1)−N(8)#2	108.3(3)	N(2)−Ag(1)−N(8)#2	106.0(3)
N(5)−Ag(2)−N(3)#3	121.0(3)	N(5)−Ag(2)−N(1)	117.4(2)
N(3)#3−Ag(2)−N(1)	110.7(3)	N(5)−Ag(2)−N(7)#4	105.4(3)
N(3)#3−Ag(2)−N(7)#4	88.9(3)	N(1)−Ag(2)−N(7)#4	108.6(3)

[a] Symmetry transformations used to generate equivalent atoms: #1 *x*, *y*, *z* − 1; #2 *x*, *y* − 1, *z* − 1; #3 *x*, *y* + 1, *z* + 1; #4 *x*, *y*, *z* + 1.

Table 7. Interatomic Distances (Å) and Bond Angles (deg) for **5**[a]

Ag(1)−N(1)	2.272(3)	Ag(1)−N(2)#1	2.297(3)
Ag(1)−N(4)#2	2.329(4)	Ag(1)−N(3)#3	2.381(4)
N(1)−Ag(1)−N(2)#1	119.44(11)	N(1)−Ag(1)−N(4)#2	120.36(14)
N(2)#1−Ag(1)−N(4)#2	103.24(14)	N(1)−Ag(1)−N(3)#3	100.73(13)
N(2)#1−Ag(1)−N(3)#3	113.61(14)	N(4)#2−Ag(1)−N(3)#3	97.57(17)

[a] Symmetry transformations used to generate equivalent atoms: #1 $-x+1, -y, -z+1$; #2 $x-1, y-1, z$; #3 $-x+1, -y+1, -z$; #4 $x+1, y+1, z$; #5 $-x, -y+1, -z+2$.

Table 8. Interatomic Distances (Å) and Bond Angles (deg) for **6**[a]

Ag(1)−N(1)	2.287(3)	Ag(1)−N(1)#1	2.287(3)
Ag(1)−N(2)#2	2.374(5)	Ag(1)−N(2)#3	2.374(5)
N(1)−Ag(1)−N(1)#1	122.24(17)	N(1)−Ag(1)−N(2)#2	119.85(17)
N(1)#1−Ag(1)−N(2)#2	98.99(17)	N(1)−Ag(1)−N(2)#3	98.99(17)
N(1)#1−Ag(1)−N(2)#3	119.85(17)	N(2)#2−Ag(1)−N(2)#3	94.8(3)

[a] Symmetry transformations used to generate equivalent atoms: #1 $-x+5/4, -y+5/4, z$; #2 $x+3/4, y-1/4, -z+1$; #3 $-x+1/2, -y+3/2, -z+1$; #4 $x, -y+5/4, -z+5/4$; #5 $-x+3/4, -y+7/4, z$; #6 $x, -y+7/4, -z+3/4$; #7 $-x+5/4, y, -z+5/4$.

Table 9. Interatomic Distances (Å) and Bond Angles (deg) for **7**[a]

Ag(1)−N(1)	2.271(6)	Ag(1)−N(2)	2.310(7)
Ag(1)−N(3)#1	2.319(9)	Ag(1)−N(4)#2	2.442(9)
N(1)−Ag(1)−N(2)	117.06(18)	N(1)−Ag(1)−N(3)#1	129.8(3)
N(2)−Ag(1)−N(3)#1	100.7(3)	N(1)−Ag(1)−N(4)#2	97.6(3)
N(2)−Ag(1)−N(4)#2	118.8(3)	N(3)#1−Ag(1)−N(4)#2	91.1(3)

[a] Symmetry transformations used to generate equivalent atoms: #1 $x-1/4, -y+5/4, z+3/4$; #2 $x+1/4, -y+5/4, z-3/4$; #3 $-x+1/2, -y+3/2$, *z*.

Table 10. Interatomic Distances (Å) and Bond Angles (deg) for **8**[a]

Ag(1)−N(1)	2.298(7)	Ag(1)−N(2)#1	2.303(8)
Ag(1)−N(3)#2	2.408(10)	Ag(1)−N(4)#3	2.434(10)
N(1)−Ag(1)−N(2)#1	123.9(3)	N(1)−Ag(1)−N(3)#2	121.4(3)
N(2)#1−Ag(1)−N(3)#2	104.0(3)	N(1)−Ag(1)−N(4)#3	96.4(3)
N(2)#1−Ag(1)−N(4)#3	117.8(3)	N(3)#2−Ag(1)−N(4)#3	88.0(3)

[a] Symmetry transformations used to generate equivalent atoms: #1 $-x+1, y, -z+1/2$; #2 $x+1, -y, z+1/2$; #3 $-x+1/2, -y+1/2, -z+1$; #4 $x-1, -y, z-1/2$; #5 $-x+1, y, -z+3/2$.

individual reaction would be determined by some parameters, for example, the templating effect of solvent molecule, the size and/or polarity of the anion, the pH value of the reaction solution, and some other subtle factors beyond the researcher's control.

Figure 2 exhibits various conformations of **L11** found in complexes **1**−**8**. As indicated in the figure, there are conformations of I, II, and versatile intermediate conformations between three fundamental conformations (I, II, and III), which suggests **L11** will generate various polymeric patterns of the resulting complexes if the solvent systems and counterions are changed. In other words, we could control the compounds' topology by means of changing reaction conditions. A typical trans conformation of III, however, was not found in this series of Ag(I)−**L11** polymeric complexes.

Synthesis of the Complexes. The slow diffusion of an organic solution (THF or CH_2Cl_2) of **L11** into a benzene solution of AgX (X = $SO_3CF_3^-$, PF_6^-, ClO_4^-, and SbF_6^-) afforded the 1:2 Ag(I)−**L11** adduct for $SO_3CF_3^-$ and a 1:1 adduct for PF_6^-, ClO_4^-, and SbF_6^-, presumably due to the different coordinating nature and templating effect of the counterions and solvent molecules.[19] All these slow-diffusion reactions are not affected by the metal-to-ligand mole ratio. Their assembled structures, however, could be determined by influencing the conformation of **L11** through the change of either the solvent intermediate or the anions. For instance, the reaction of $AgSO_3CF_3$ with **L11** in a THF/benzene or CH_2Cl_2/benzene system produced a one-dimensional zigzag chain structure, whereas the treatment of $AgPF_6$ (THF/benzene), $AgClO_4$ (CH_2Cl_2/benzene), or $AgSbF_6$ (THF/benzene) with **L11** gave a two-dimensional network; the reaction of $AgClO_4$ (THF/benzene), $AgBF_4$ (THF/benzene), or $AgSbF_6$ (THF/benzene) with **L11** afforded a three-dimensional network. As depicted in Figure 2, in one-dimensional compounds **1** and **2**, **L11** adopts conformation II, in which the central oxadiazole group and its two adjacent phenyl rings are basically coplanar. The dihedral angles between the central oxadiazole and two neighboring phenyl rings lie in the ranges of 3.76−4.39° and 3.87−5.69°, respectively. In two-dimensional compounds **3**−**5**, **L11** takes either conformation I or II, with dihedral angles between the central oxadiazole and two neighboring phenyl rings of 23.51−34.29° and 23.94−33.64°, respectively. In three-dimensional compounds **6**−**8**, **L11** chooses an intermediate conformation between I and III, with the two long cyanophenylacetylene arms lying in the different planes. The dihedral angles between the two long arms attached to the central oxadiazole are 59.80° (**6**), 49.16° (**7**), and 57.94° (**8**). All the crystalline solids are not soluble in water or common

(18) To gain a deeper insight into the coordination behavior of this type of ligands, we performed ab initio Mulliken population analysis on ligand **L11.** The calculation results of **L11** show that the energies of three possible conformations of **L11** in either gas or benzene solution are almost identical. Thus, these three conformations, I, II, and III, could be concomitant in gas or benzene solution.

(19) (a) Raehm, L.; Mimassi, L.; Guyard-Duhayon, C.; Amouri, H. *Inorg. Chem.* **2003**, *42*, 5654. (b) Pike, R. D.; Borne, B. D.; Maeyer, J. T.; Rheingold, A. L. *Inorg. Chem.* **2002**, *41*, 631. (c) Prior, T. J.; Rosseinsky, M. J. *Inorg. Chem.* **2003**, *42*, 1564. (d) Jung, O.-K.; Kim, Y. J.; Lee, Y.-A.; Park, K.-M.; Lee, S. S. *Inorg. Chem.* **2003**, *42*, 844. (e) Platas-Lglesias, C.; Esteban, D.; Ojea, V.; Avecilla, F.; de Blas, A.; Rodringuez-Blas, T. *Inorg. Chem.* **2003**, *42*, 4299. (f) Wu, B.; Yuan, D.; Lou, B.; Han, L.; Liu, C.; Zhang, C.; Hong, M. *Inorg. Chem.* **2005**, *44*, 9175. (g) Fletcher, A. J.; Cussen, E. J.; Prior, T. J.; Rosseinsky, M. J.; Kepert, C. J.; Thomas, K. M. *J. Am. Chem. Soc.* **2001**, *123*, 10001.

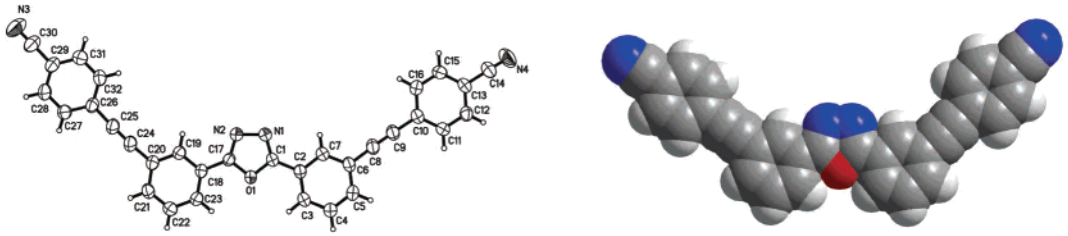

Figure 1. Molecular structure of **L11**: ORTEP (right) and space-filling (left) figures.

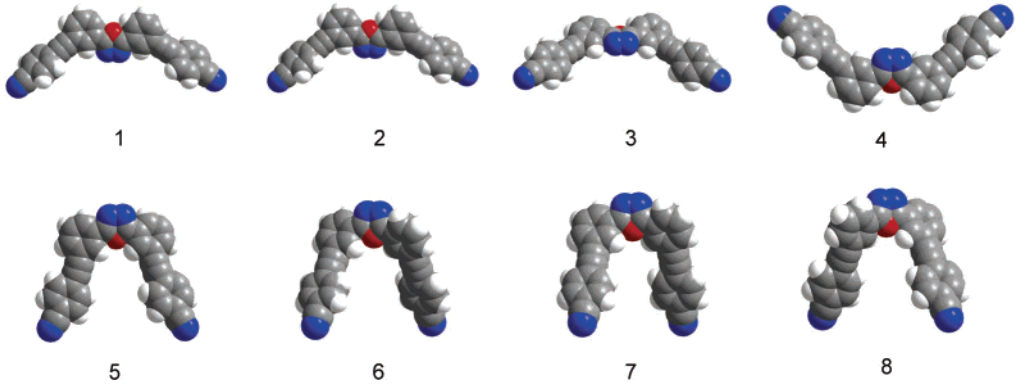

Figure 2. Various conformations of **L11** found in **1**−**8**.

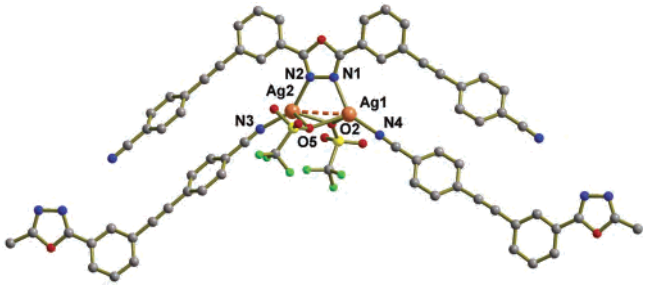

Figure 3. Coordination environment of Ag(I) in **1.**

organic solvents because of their polymeric nature but are dissolved by CH_3CN and DMSO.

Structural Analysis. One-Dimensional Complexes of $[Ag_2(L11)(SO_3CF_3)_2]\cdot(C_6H_6)$ (1) and $Ag_2(L11)(SO_3CF_3)_2]\cdot(C_6H_6)$ (2). Crystallization of **L11** with $AgSO_3CF_3$ in a CH_2Cl_2/C_6H_6 mixed-solvent system at room temperature afforded compound **1** as an infinite one-dimensional chain structure in 55% yield. Single-crystal analysis revealed that there are two crystallographic independently Ag(I) centers in **1**. Both kinds of Ag(I) atoms adopt a $\{AgN_2O_2\}$ coordination sphere. As shown in Figure 3, two different Ag(I) atoms are bound together by two $N_{oxadiazole}$ donors on the central oxadiazole ring of **L11** and two $O_{triflate}$ donors into a $\{Ag_2O_2N_2\}$ cluster core in which the Ag(1)···Ag(2) distance is ∼3.5 Å, which is comparable to the sum of the van der Waals radii of two silver atoms, 3.44 Å. In the solid state, ligand **L11** adopts conformation II and acts as a tetradentate spacer to link Ag(I) atoms into a one-dimensional zigzag double-chain structure with the bending angle ca. 132° extended along the crystallographic [0$\bar{1}$1] direction (Figure 4). In the double chain, two ethynylbenzonitrilephenyl arms are doubling-up and parallel to each other, leading to the interchain $\pi-\pi$ interactions (centroid-to-centroid distance of ca. 3.9 Å).[20] These zigzag double chains stack offset, generating channels (Figure 5) in which two columns of benzene solvent molecules are located as the guest. When viewed down the crystallographic *a* and *b* axes, almost-regular rectangular and parallelogram-like channels (effective cross section of ca. 10 × 13 Å^2 and 10 × 12 Å^2, respectively) were found. Inside the channels, benzene molecules and $SO_3CF_3^-$ counterions are located (Figure 6).

Scheme 3. Three Typical Possible Conformations of **L11**

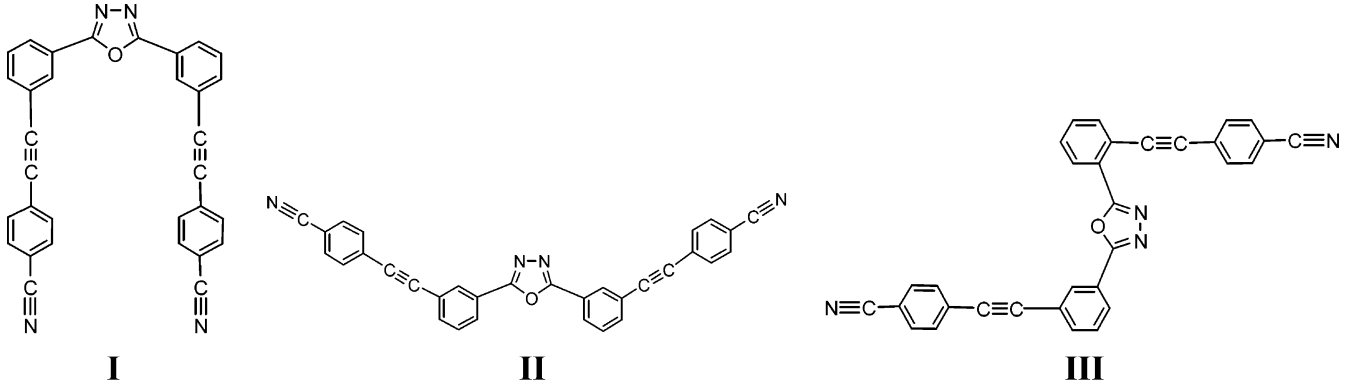

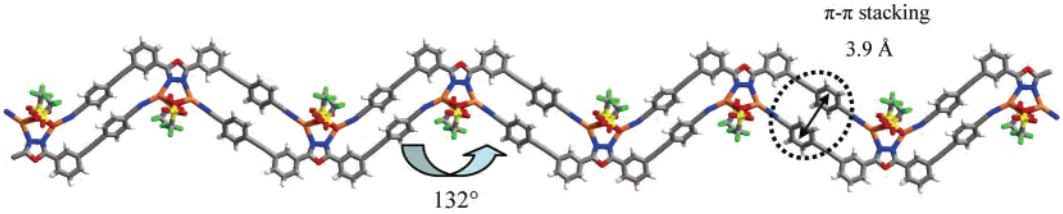

Figure 4. One-dimensional zigzag double chain of **1**.

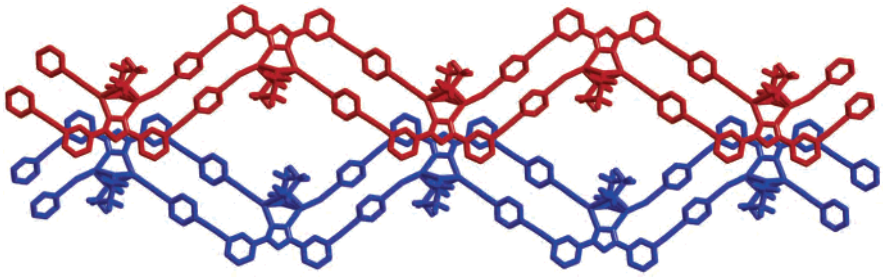

Figure 5. Representation of how the channel forms. Two sets of one-dimensional chains are given in different colors for clarity.

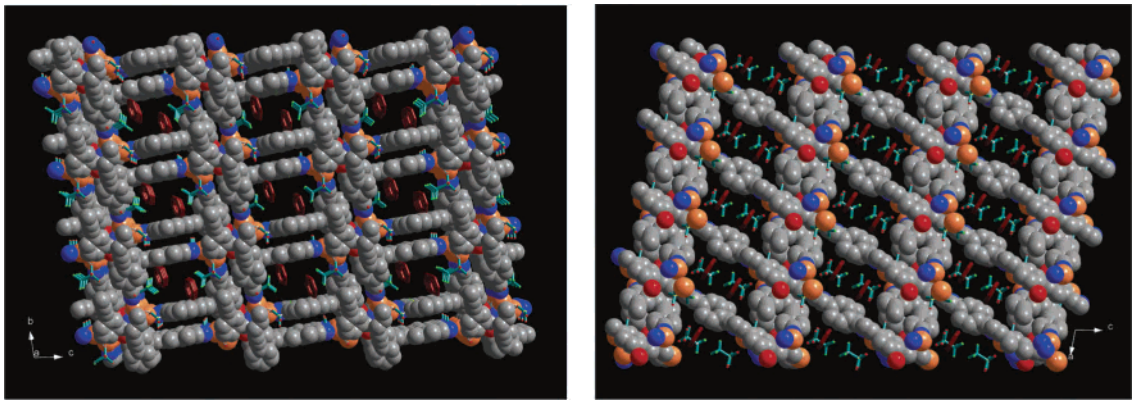

Figure 6. Spacing-filling representation of **1** showing channels along the crystallographic *a* (left) and *b* (right) axes. The $SO_3CF_3^-$ anion and benzene guest molecule are shown in the stick−ball mode.

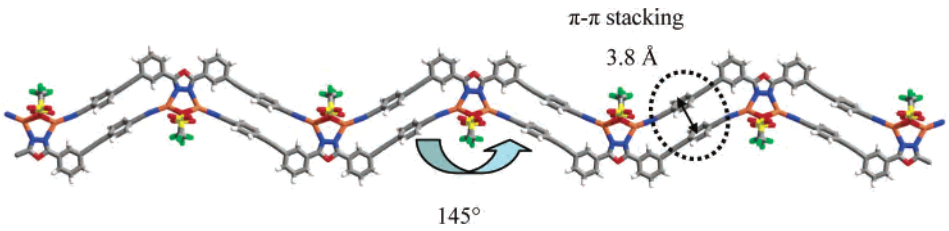

Figure 7. One-dimensional zigzag double chain of **2**.

Complex $[Ag_2(\mathbf{L11})SO_3CF_3]_2 \cdot C_6H_6$ (**2**) was obtained from a THF/benzene mixed-solvent system. **2** is composed of the similar one-dimensional double-zigzag Ag−**L11** chain with the same intrachain $\pi-\pi$ interaction as **1** (Figure 7). It is likely the different solvent intermediates gave rise to the slight change in the ligand's conformation, which lies in the fact that the dihedral angles between the two phenyl rings on the same ethynylbenzonitrilephenyl arm changed from 33.46 and 43.59° in **1** to 69.35 and 69.59° in **2**, respectively. Such changes could be what leads to the larger bending angle of the zigzag chain in **2** (145°) and successively affects the crystal-stacking fashion in the solid state. As indicated in Figure 8, when viewed down the crystallographic *a* axis, the coordination $SO_3CF_3^-$ anions occupied the parallelogram channels and the benzene solvent molecules are covered by the framework; when viewed down the crystallographic *b* axis, both $SO_3CF_3^-$ anions and benzene molecules are visible in the parallelogram-like channels but with a different orientation compared to that of **1**.

In the structures of both **1** and **2**, the $SO_3CF_3^-$ anion acts as a $\mu-\eta^1$ bridging ligand [21] rather than the $\mu-\eta^2$ bridging, terminal, or chelating coordination mode commonly observed

(20) Chen, C.-L.; Su, C.-Y.; Cai, Y.-P.; Zhang, H.-X.; Xu, A.-W.; Kang, B.-S.; zur Loye, H.-C. *Inorg. Chem.* **2003**, *42*, 3788.

(21) (a) Eisler, D. J.; Puddephatt, R. J. *Cryst. Growth Des.* **2005**, *5*, 57. (b) Awaleh, M. O.; Badia, A.; Brisse, F.; *Cryst. Growth Des.* **2005**, *5*, 1897. (c) Schultheiss, N.; Powell, D. R.; Bosch, E. *Inorg. Chem.* **2003**, *42*, 8886. (d) Eisler, D. J. Puddephatt, R. J. *Inorg. Chem.* **2005**, *44*, 4666. (e) Custer, P. D.; Garrison, J. C.; Tessier, C. A.; Yongs, W. *J. Am. Chem. Soc.* **2005**, *127*, 5738. (f) Brandys, M.-C.; Puddephatt, R. J. *J. Am. Chem. Soc.* **2002**, *124*, 3946.

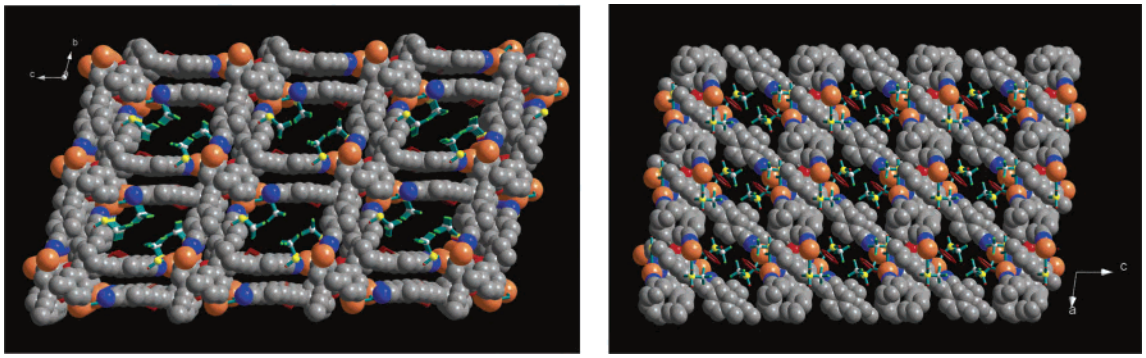

Figure 8. Crystal packing of **2** down the crystallographic *a* (left) and *b* (right) axes.

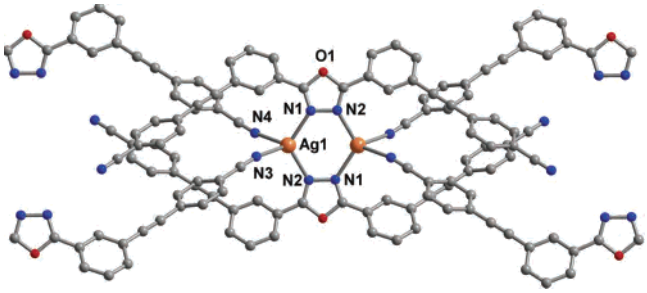

Figure 9. Coordination sphere of Ag(I) in **3**.

in many other Ag−triflate complexes.[14,21] Such a $\mu-\eta^1$ coordinated triflate anion, however, has been structurally characterized for the first time in our bent ligand−silver triflate system.[14] The $\mu-\eta^1$ coordinating mode would result in the relatively small O−Ag−O bond angles (76.33(16)−79.54 (18)° in **1** and **2**), which leans to the formation of the sterically hindered cluster core being unfavorable in the self-assembly process.

Two-Dimensional Complexes. [Ag(L11)]PF_6 (3). Compound **3** was prepared by reacting **L11** with a stoichiometric amount of $AgPF_6$ in the same mixed-solvent system as that in **2**. It is different from compounds **1** and **2** in that **3** presents a noninterpenetrating two-dimensional network in the solid state. As shown in Figure 9, there is only one type of Ag(I) center in **3**. Compared to those of **1** and **2**, the coordination sphere of the Ag(I) atom changed from $\{AgO_2N_2\}$ to $\{AgN_4\}$, which is clearly caused by changing the coordinated $SO_3CF_3^-$ to an uncoordinated PF_6^- anion. The $\{AgN_4\}$ sphere is composed of two $N_{oxadiazole}$ (Ag(1)−N = 2.282(5) Å) and two $N_{nitrile}$ donors (Ag(1)−N(3) = 2.364(7) and Ag-(1)−N(4) = 2.418(8) Å). Two central oxadiazole groups bind two Ag(I) atoms through four oxadiazole N donors to generate a $\{Ag_2N_2\}$ bimetallic ring, in which the Ag···Ag distance is 3.7 Å. Such a bimetallic silver ring was observed in our previous studies on L1−L10.[14] Four $\{Ag_2N_4\}$ moieties are doubly connected to each other by the ethynylbenzonitrilephenyl arms of the tetradentate **L11** ligands, generating a rhombuslike molecular cage, in which the two pairs of opposite Ag···Ag distances are ca. 12 and 27 Å, respectively. As shown in Figure 10, each terminal benzonitrile ring of the ethynylbenzonitrilephenyl linkage is parallel to that of an adjacent ethynylbenzonitrilephenyl segment, resulting in interligand $\pi-\pi$ interactions (centroid-to-centroid distance between two benzene groups of ca. 3.9 Å). As depicted in

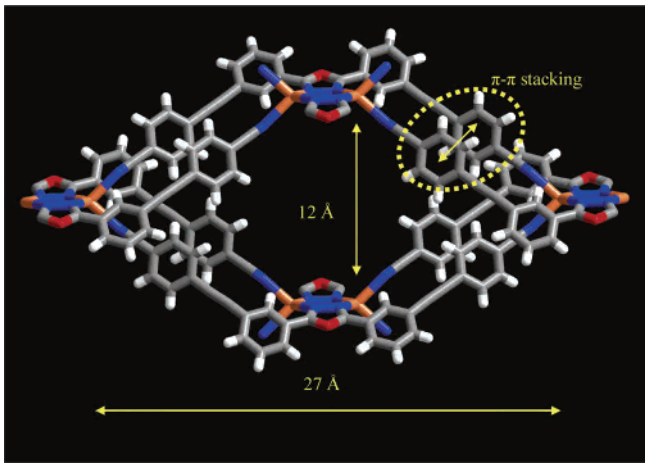

Figure 10. Molecular cage found in **3**. The two uncoordinated PF_6^- anions are omitted for clarity.

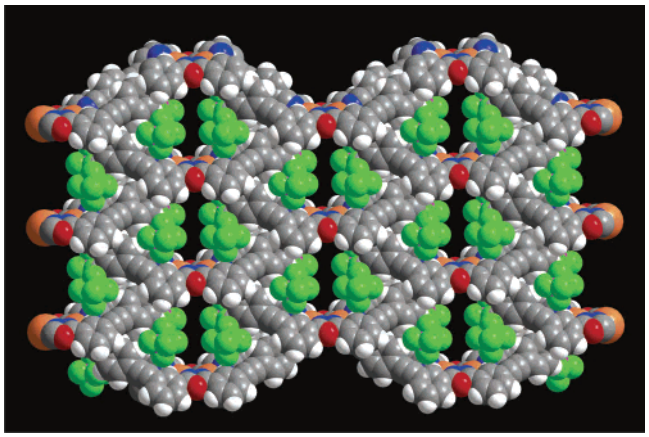

Figure 11. Space-filling view of the two-dimensional net containing PF_6^- anions in **3**.

Figure 11, the two-dimensional net is extended in the crystallographic *bc* plane. All of the two-dimensional nets stack along the crystallographic *a* axis, generating rhombic channels in which two columns of PF_6^- anions are arranged into an approximately linear array that fits tightly into the phenyl rings surrounding the central cavity. In addition, each PF_6^- counterion is hydrogen bonded to the two adjacent layers through F···H−C hydrogen bonds and is linked together along the crystallographic *a* axis, giving rise to a three-dimensional hydrogen-bonded network (Figure 12). The F···H−C hydrogen bond lengths fall within the range of 2.2−2.5 Å.[22]

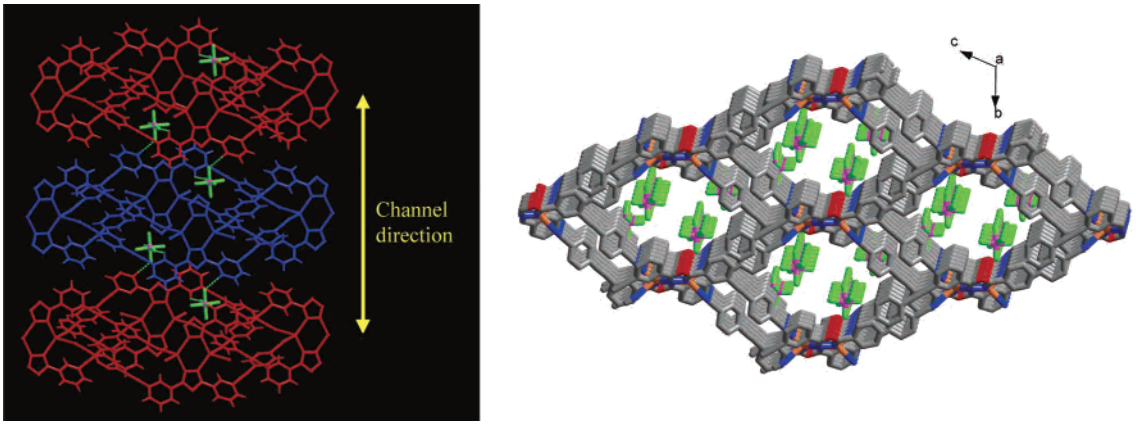

Figure 12. PF_6^- anion links two-dimensional nets into an H-bonded three-dimensional framework. Three layers are shown in different colors for clarity. F···H−C hydrogen bonds are shown as green dotted lines (left). H-bonded networks with rhombic channels along the crystallographic *a* axis (right).

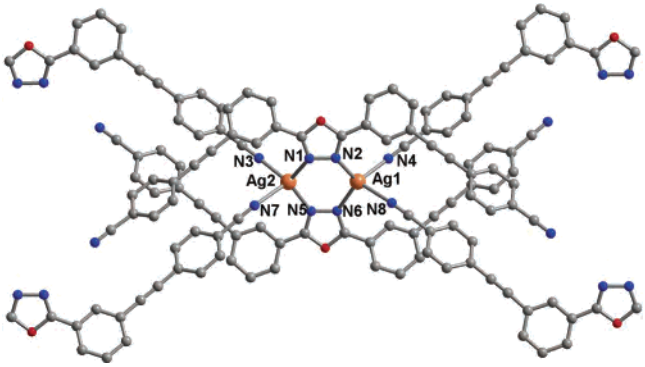

Figure 13. Coordination sphere of Ag(I) in **4**.

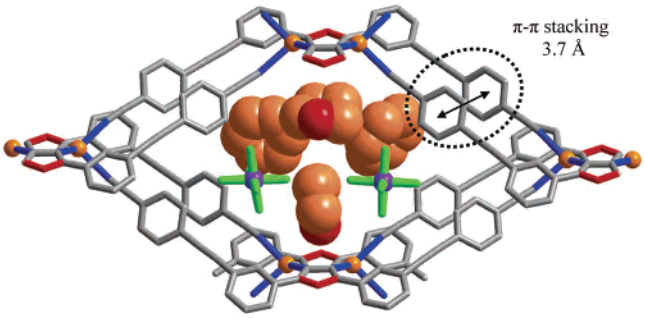

Figure 14. Molecular Ag(I)−**L11** cage in **4**. The benzene and THF solvent molecules are shown in the space-filling mode.

A series of two-dimensional Ag(I)X−L8 polymeric coordination complexes (X = BF_4^-, SbF_6^-, and $SO_3CF_3^-$) containing a similar molecular-cage-like building unit has been reported by us recently. Therein, the dimensions of the rhombic molecular cage are only ca. 8 × 16 Å^2.[14] As shown above, the Ag(I)−**L11** molecular cage is successfully enlarged by the use of a longer organic spacer without interpenetration or self-inclusion.[23]

[Ag(L11)]SbF_6·(C_6H_6)·(THF) (4). To explore the templating effect[19] of the counterion on the long-range order of the Ag(I)−**L11** coordination polymer, we used the larger-sized SbF_6^- anion instead of the PF_6^- anion. Crystallization of **L11** with $AgSbF_6$ in the same THF/benzene solvent system at room temperature produced an infinite noninterpenetrating two-dimensional polymeric compound **4** as blocklike colorless crystals. In **4**, **L11** adopts the same conformation as that of **3**. Both crystallographically independent Ag(I) centers lie in the same {AgN_4} distorted tetrahedral coordination sphere (Figure 13), which is similar to that of compound **3**. The Ag−N bond lengths lie in the range of 2.278−2.499 Å. Two of the Ag−$N_{nitrile}$ bond distances (Ag−N(7) and Ag−N(8)) are slightly longer that those corresponding bond lengths in **3**. The same rhombus-like molecular cage based on {Ag_2N_4} connecting nodes with the same dimensions has been found. Compared to the molecular cage in **3**, the $\pi-\pi$ interactions between the two adjacent frame rungs is stronger, which is manifested in a shorter centroid-to-centroid distance (3.7 Å) (Figure 14). It is different from **3**; the molecular cage herein is full of benzene and THF guest molecules besides SbF_6^- anions, which could be the reason that crystals of **4** turn opaque within minutes under an ambient atmosphere. The existence of benzene and THF molecules were further confirmed by the NMR spectrum. In the ^{1}H NMR (in DMSO) spectrum of **4**, proton resonances were observed at 7.37 (singlet) ppm and 3.53 and 1.73 (triplets) ppm, which were attributed to benzene and the THF guest molecule, respectively.

4 features a stacking fashion similar to that of **3**, which generates the rhombic channels along the crystallographic *a* axis. Two columns of benzene and two columns of THF molecules are located in the channels (Figure 15). The accessible void volume of the channels in one unit cell is 872.1 Å^3, which is estimated to be 43.7% of the total volume (1995.0 Å^3). It is worth pointing out that compound **4** crystallizes in the chiral triclinic space group *P*1, an enantiomorphous space group confirmed on the basis of an absolute structure (Flack) parameter of 0.00 from the X-ray data. At this stage, we could not explain the chirality-forming mechanism of **4** by simply changing PF_6^- in **3** to SbF_6^- in **4**. Nevertheless, compound **4** herein affords an additional example of a chiral polymeric complex obtained by the spontaneous resolution on crystallization with achiral auxiliary.[24] The existence of this chiral and porous system

(22) (a) Braga, D.; Grepioni, F.; Desiraju, G. R. *Chem. Rev.* **1998**, *98*, 1375. (b) Shimoni, L.; Carrell, H. L.; Glusker, J. P.; Coombs, M. M. *J. Am. Chem. Soc.* **1994**, *116*, 8162.

(23) The longer ligands would favor the formation of interpenetrating over noninterpenetrating structures: Batten, S. R.; Robson, R. *Angew. Chem., Int. Ed.* **1998**, *37*, 1460.

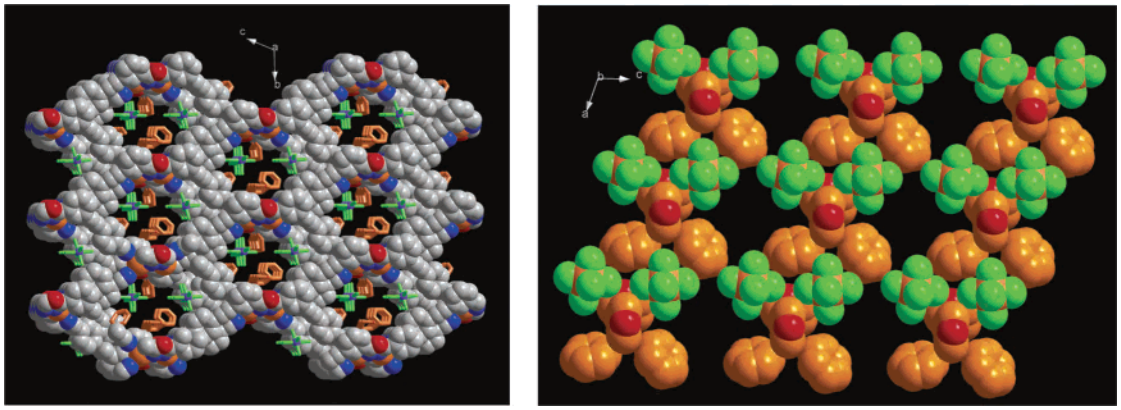

Figure 15. Crystal packing (left) and solvent and PF_6^- arrangement (right) found in **4**.

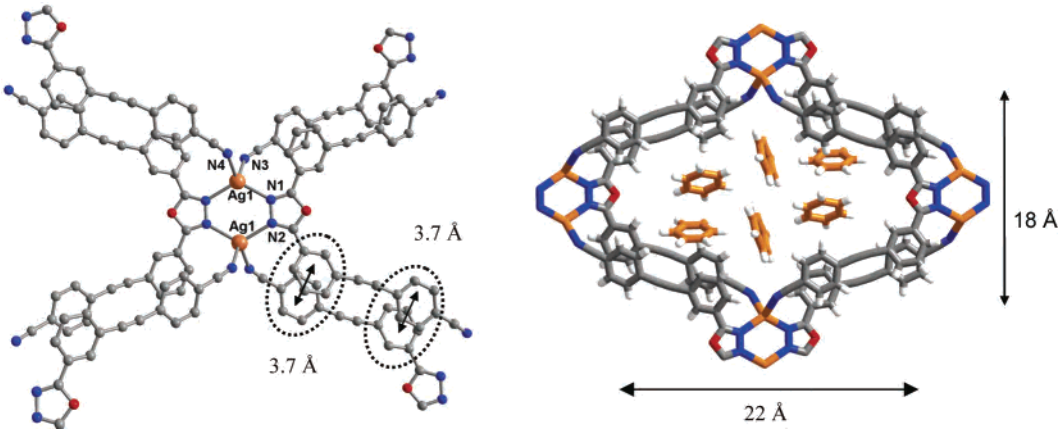

Figure 16. Coordination environment of Ag(I) (left) and metalla-macrocycle (right) in **5**.

suggests opportunities for the chiral selectivity of host molecules and potentially even chiral selectivity for reactions that might benefit from taking place inside spatially confined channels and its local chemical microenvironment.

[Ag(L11)ClO$_4$]·2.5(C$_6$H$_6$) (5). Combining $AgClO_4$ and **L11** in a CH_2Cl_2/benzene mixed-solvent system generated compound **5** as a colorless blocklike crystal (Yield, 51%). In **5**, **L11** adopts conformation I instead of conformation II, as seen in complexes **3**−**4**. In contrast to conformation II, two long ethynylbenzonitrilephenyl arms rotate ca. 180° around *exo*-oxadiazole carbon−carbon single bonds and point in the same direction, leading to a Π-shaped spacer. As shown in Figure 16, the Ag(I) atom again adopts a distorted tetrahedral coordination sphere and the $\{Ag_2N_4\}$ cluster nodes are doubly connected to form an approximately rhombus-shaped metalla-macrocycle through two sets of parallel ethynylbenzonitrilephenyl linkages. The distances between the two opposite pairs of silver ions on the macrocycle are ∼18 and ∼22 Å. Again, each of the macrocyclic sides is reinforced by the interligand $\pi-\pi$ interaction. Six benzene solvent molecules are located in the macrocyclic cavity. In **5**, the $\{Ag_2N_4\}$ plane is nearly parallel to the macrocyclic ring, whereas it projects perpendicularly to the cage plane in **3** and **4**. The different orientation of the $\{Ag_2N_4\}$ plane is clearly caused by the different conformations adopted by **L11** in these complexes. As shown in Figure 17, the macrocyclic structure of **5** propagates along two dimensions, resulting in the generation of a two-dimensional layer. These two-dimensional layers are arranged in the crystal in an AB−AB fashion resembling that of rhombic close packing, such that the macrocyclic cavity does not exhibit extended channels. Although such a stacking arrangement effectively reduces the void volume present in the structure, an inspection of Figure 18 reveals that the overall array contains a three-dimensional intersecting channel system and nanoscale open windows, with an approximate effective cross section of ca. 14 × 9 Å^2 (down *a*), 15 × 10 Å^2 (down *b*), and 12 × 16 Å^2 (down *c*), which is reflected in a large solvent-accessible volume of 898.0 Å^3 (47.5% of a total unit-cell volume of 2082.1 Å^3). Solvent molecules are found in the different channel space with different orientations. There are no significant interactions between the solvent molecules and the host framework.

The common feature of two-dimensional complexes **3**−**5** is the coplanarity of the two long ethynylbenzonitrilephenyl arms attached to a central oxadiazole ring, no matter which conformation (I or II) **L11** adopts. Second, the **L11** spacer doubles up and the $\{Ag_2N_2\}$ cluster core is the connecting node in the framework, which gives rise to the formation of the double-decked layer. More importantly, such connectivity

(24) (a) Katsuki, I.; Motoda, Y.; Sunatsuki, Y.; Matsumoto, N.; Nakashima, T.; Kojima, M. *J. Am. Chem. Soc.* **2002**, *124*, 629. (b) Gao, E.-B.; Bai, S.-Q.; Wang, Z.-M.; Yan, C.-H. *J. Am. Chem. Soc.* **2003**, *125*, 4984. (c) Sasa, M.; Tanaka, K.; Bu, X.-H.; Shiro, M.; Shionoya, M. *J. Am. Chem. Soc.* **2001**, *123*, 10750.

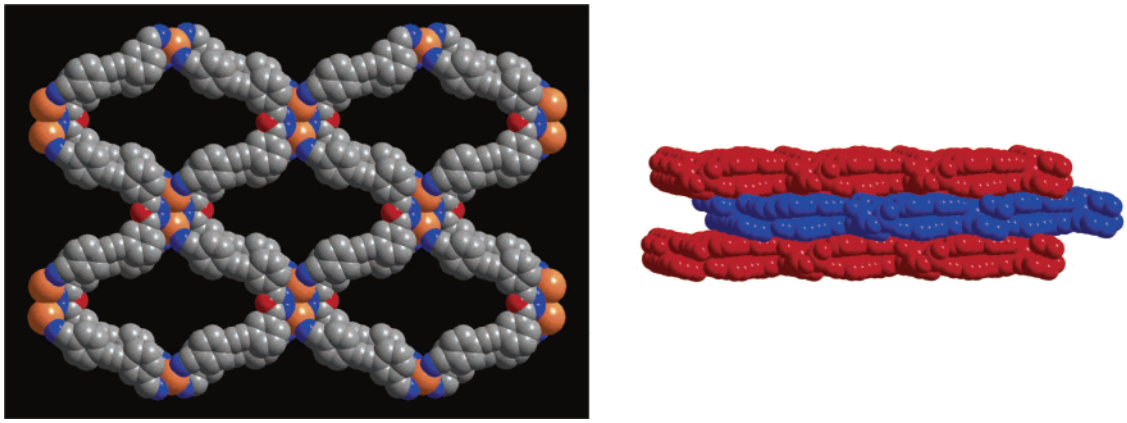

Figure 17. Top view of the two-dimensional net with rhombic cavity (left) and side view of the AB−AB stacking fashion (right) found in **5**. Two sets of sheets are represented by the red and blue colors in the figure.

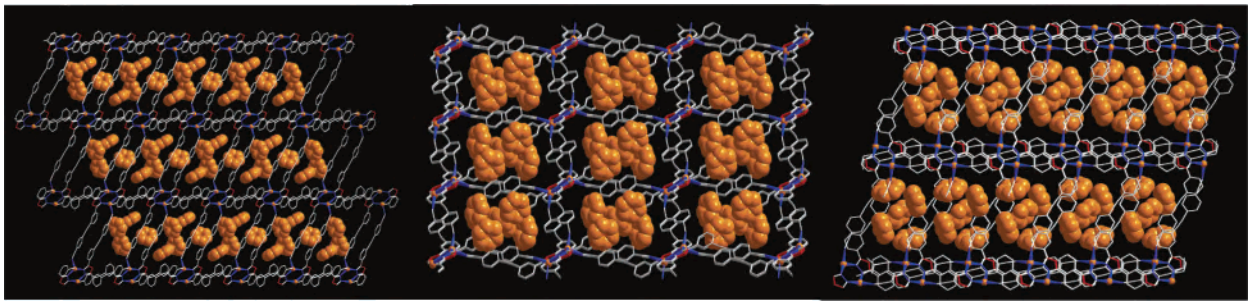

Figure 18. Ball−stick representation of **5** showing channels opening along the crystallographic *a*, *b*, and *c* axes (from left to right). The benzene solvent molecules are shown in the spacing-filling mode.

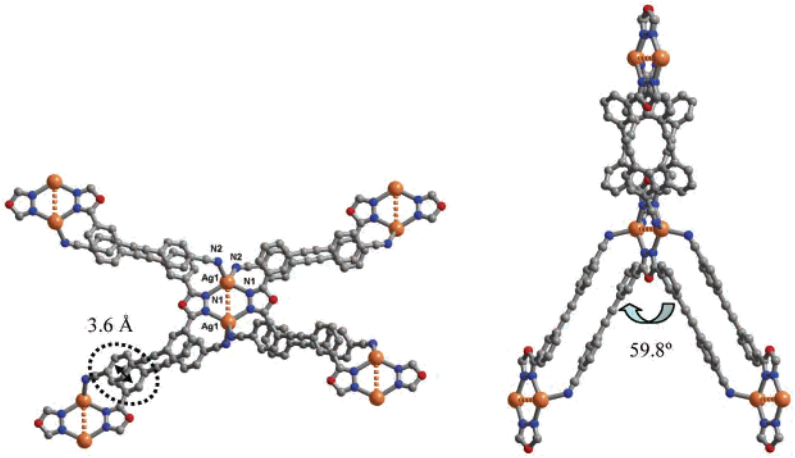

Figure 19. Four-connected $\{Ag_2N_4\}$ cluster core being doubly linked by **L11** into a tetrahedral building block.

effectively prevents the molecule's solid-state packing from interpenetration or self-inclusion and enables the formation of large rhombic grids with infinite channels.

Three-Dimensional Complexes. [Ag(L11)]BF_4·2.5(C_6H_6) (6) and [Ag(L11)]SbF_6·unknown solvate (7). Combining **L11** with $AgBF_4$ in a THF/benzene mixed-solvent system at room temperature generated compound **6** as a colorless crystal in 51% yield. X-ray single-crystal analysis revealed that compound **6** crystallizes in the orthorhombic space group *Fddd*. The silver atom lies in a distorted coordination sphere consisting of four N donors from two terminal benzonitrile groups and two central oxadiazole rings. As shown in Figures 3 and 19, **L11** adopts the intermediate conformation between I and III (with the dihedral angle between the two ethynylbenzonitrilephenyl arms being ca. 60°) and binds two Ag(I) ions in a back-to-back fashion through the Ag(I)−$N_{oxadiazole}$ interaction. This gives rise to a $\{Ag_2N_4\}$ cluster core upon which four ethynylbenzonitrilephenyl arms stretch outward in four different directions, leading to the formation of a tetrahedral building block. The intracore Ag···Ag distance is 3.5 Å, which is comparable to that of **1** and indicative of little direct metal−metal interaction. As indicated in Figure 20a, the assembly of a tetrahedral building block results in a three-dimensional adamantoid arrangement that leaves a huge cavity inside the framework. The three pairs of intracage diagonal Ag···Ag distances across the individual adamantoid are 57, 44, and 38 Å. Two terminal benzonitrile rings of each ethynylbenzonitrilephenyl linkage are basically

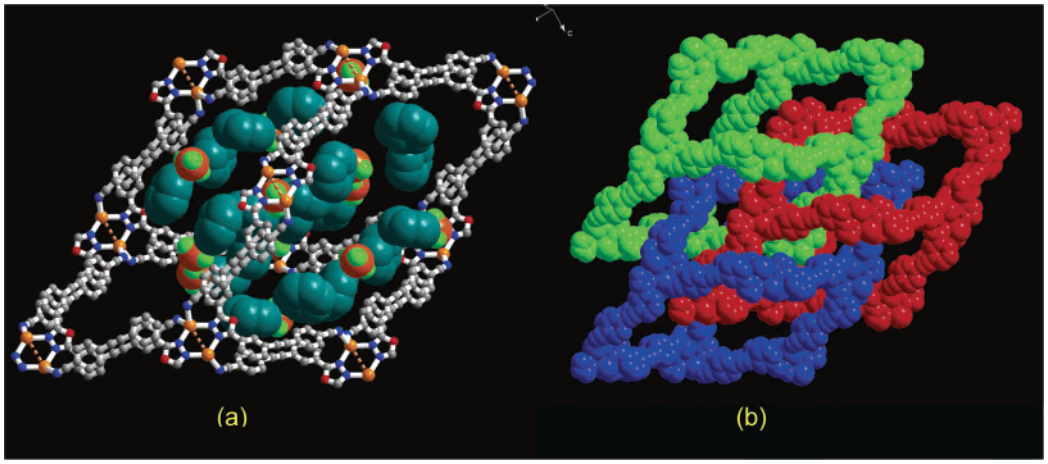

Figure 20. (a) Ball and stick representation of single adamantoid cage formed in an individual framework. Benzene and anion guests are shown in the space-filling mode. (b) Space-filling illustration of how three frameworks in **6** interpenetrate. The three independent frameworks are colored red, green, and blue.

coplanar and are parallel to those of adjacent ethynylbenzonitrilephenyl segments, again resulting in interligand $\pi-\pi$ interactions (a centroid-to-centroid distance between two benzene groups of ca. 3.6 Å). Such an arrangement, beyond all doubt, reinforces the host cage. The remarkable feature of **6** is that the adamantoid cage is capped by the $\{Ag_2N_4\}$ cluster core instead of simple silver ions being connecting nodes, which is rarely observed otherwise;[25,26] Second, the adamantoid framework is doubly pinned up by the ligand. To the best of our knowledge, such adamantoid construction of **1** is unprecedented (Chart 3). When viewed down the crystallographic *a*, *b*, [101], and [0$\bar{1}$1] directions, huge honeycomb- (31 × 27 Å^2), ellipse- (23 × 14 Å^2), square- (18 × 24 Å^2), and rhombuslike (36 × 13 Å^2) channels have been found (Figure 21), respectively. Unfortunately, these channels of an individual diamondoid framework are partially filled by two other interpenetrated symmetry-equivalent frameworks, leading to a 3-fold interpenetrated structure (Figure 20b). In the case of **6**, the 3-fold interpenetration of the framework generates reduced, yet still very large, infinite regular honeycomb and semicircular channels along the crystallographic *a* and [110] directions with dimensions of ca. 16 × 15 and 10 × 8 Å^2, respectively (Figure 22), in which the BF_4^- anions and benzene molecules are located as guests. The solvent-accessible volume calculated with the PLATON program is 6556.7 Å^3, which accounts for ca. 40% of the crystal volume (16474.0 Å^3).

Chart 3. Common (left) and New (right) Adamantoid Frameworks[a]

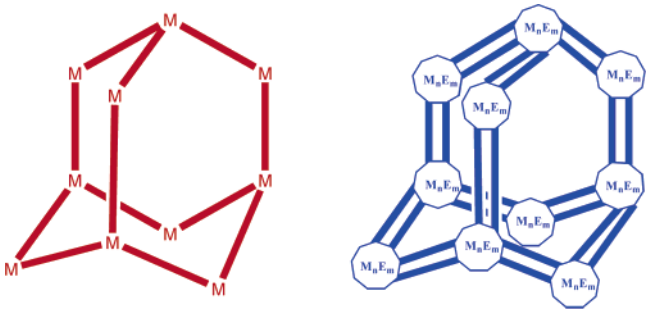

[a] The common framework consists of a simple metal ion node and a single-linked spacer. The new adamantoid framework is composed of a cluster core node, shown as M_nE_m and a double-linked space.

Compound **7** was obtained from the same reaction as that used for the preparation of **4** as colorless crystals. It seems to us that both **4** and **7** were constructed simultaneously during the reaction. The shape and color of the crystals of **7** are same as those of **4**; thus, we could not separate them manually. X-ray single-crystal analysis revealed that the given silver atom adopts the same coordination environment as **6** (Figure 23) and that **7** exhibits a 3-fold interpenetrating diamondoid coordination framework similar to that of **6** (Figure 24). A diamondoid cage of **7** (overall dimensions are almost identical to those of **6**; the intracage opposite Ag···Ag diagonal distances across the individual adamantoid are 5.7 × 4.5 × 4.1 nm^3) is capable of encapsulating SbF_6^- anion, benzene, and THF guest molecules.[27] Calculation

(25) For earlier examples of diamondoid frameworks, see: (a) MacGillivray, L. R.; Subramamian, S.; Zaworotko, M. J. *J. Chem. Soc., Chem. Commun.* **1994**, 1325. (b) Proserpio, D. M.; Hoffmann, R.; Preuss, P. *J. Am. Chem. Soc.* **1994**, *116*, 9634. (c) Batten, S. R.; Robson, R. *Angew. Chem., Int. Ed.* **1998**, *37*, 1461. (d) Zaworotko, M. J. *Chem. Soc. Rev.* **1994**, 283. (e) Lopez, S.; Kahraman, M.; Harmata, M.; Keller, S. W. *Inorg. Chem.* **1997**, *36*, 6138. (f) Blake, A. J.; Champness, N. R.; Chung, S. S. M.; Li, W.-S.; Schröder, M. *Chem. Commun.* **1997**, 1005. (g) Michaelides, A.; Kiritsis, V.; Skoulika, S.; Aubry, A. *Angew. Chem., Int. Ed.* **1993**, *32*, 1495. (h) Hirsch, K. A.; Venkataraman, D.; Wilson, S. R.; Moore, J. S.; Lee, S. *Chem. Commun.* **1995**, 2199. (i) Hirsch, K. A.; Wilson, S. R.; Moore, J. S. *Chem.—Eur. J.* **1997**, *3*, 765. (k) Hirsch, K. A.; Wilson, S. R.; Moore, J. S. *Inorg. Chem.* **1997**, *36*, 2960. (l) Munakata, M.; Wu, L. P.; Yamamoto, M.; Kuroda-Sowa, T.; Maekawa, M. *J. Am. Chem. Soc.* **1996**, *118*, 3117. (m) Sinzger, K.; Hünig, S.; Jopp, M.; Bauer, D.; Bietsch, W.; von Schütz, J. U.; Wolf, H. C.; Kremer, R. K.; Metzenthin, T.; Bau, R.; Khan, S. I.; Lindbaum, A.; Langauer, C. L.; Tillmanns, E. *J. Am. Chem. Soc.* **1993**, *115*, 7696.

(26) Several diamondoid frameworks based on cluster connecting nodes have been reported very recently: (a) Liang, K.; Zheng, H.; Song, Y.; Lappert, M. F.; Li, Y.; Xin, X.; Huang, Z.; Chen, J.; Lu, S. *Angew. Chem., Int. Ed.* **2004**, *43*, 5776. (b) Cheng, J.-K.; Chen, Y.-B.; Wu, L.; Zhang, J.; Wen, Y.-H.; Li, Z.-J.; Yao, Y.-G. *Inorg. Chem.* **2005**, *44*, 3386. (c) Liang, J.-P.; Xu, Q.-F.; Yuan, R.-X.; Abrahams, B. F. *Angew. Chem., Int. Ed.* **2004**, *43*, 4741. (d) Hoffart, D. J.; Cote, A. P.; Shimizu, G. K. H. *Inorg. Chem.* **2003**, *42*, 8603. (e) Wang, X.-S.; Zhao, H.; Qu, Z.-R.; Ye, Q.; Zhang, J.; Xiong, R.-G.; You, X.-Z.; Fun, H.-K. *Inorg. Chem.* **2003**, *42*, 5786.

(27) Nnumerous electron-density peaks were observed in the large voids between the 3-fold interpenetrating $[Ag(\mathbf{L11})]^+$ frameworks. The single peak at 7.36 and triple peaks at 3.32 and 1.76 ppm in the ^{1}H NMR spectrum of **2** indicate that the crystallographically unknown solvent molecules are benzene and THF.

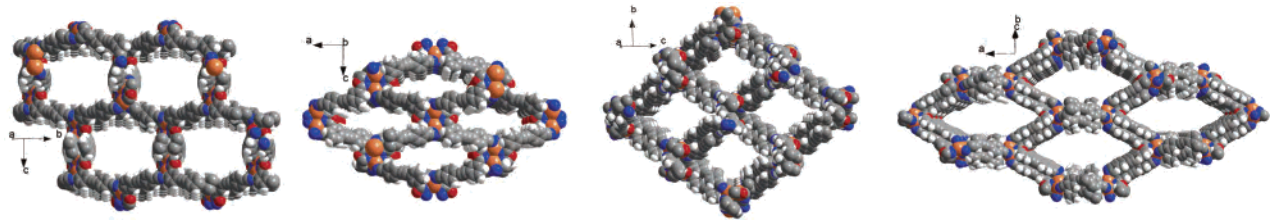

Figure 21. Space-filling diagrams of **6** viewed down the *a*, *b*, [101], and [0$\bar{1}$1] crystallographic directions.

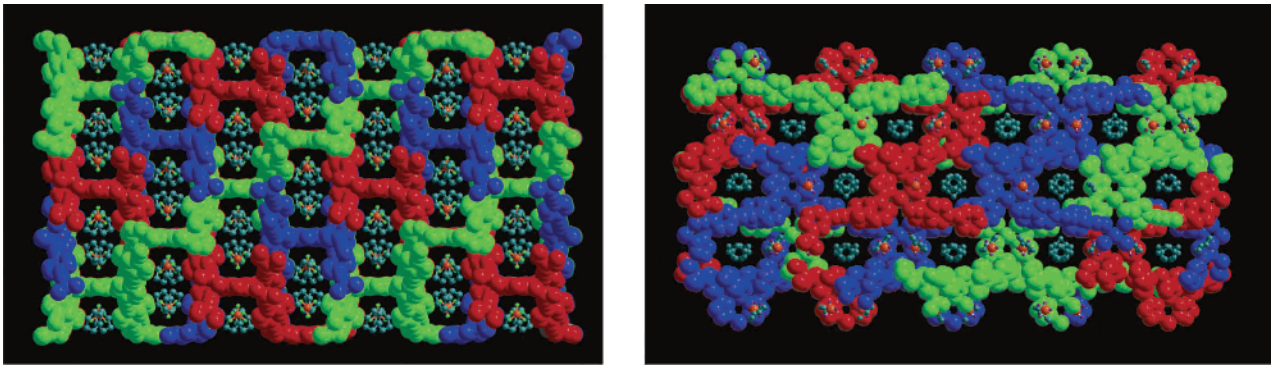

Figure 22. Three-fold interpenetration showing the hexagonal (viewed down the *a* axis, top) and semicircular (viewed down the [110] direction, bottom) channels. Frameworks are shown as space-filling models, and three sets of diamondoid frameworks are shown as different colors.

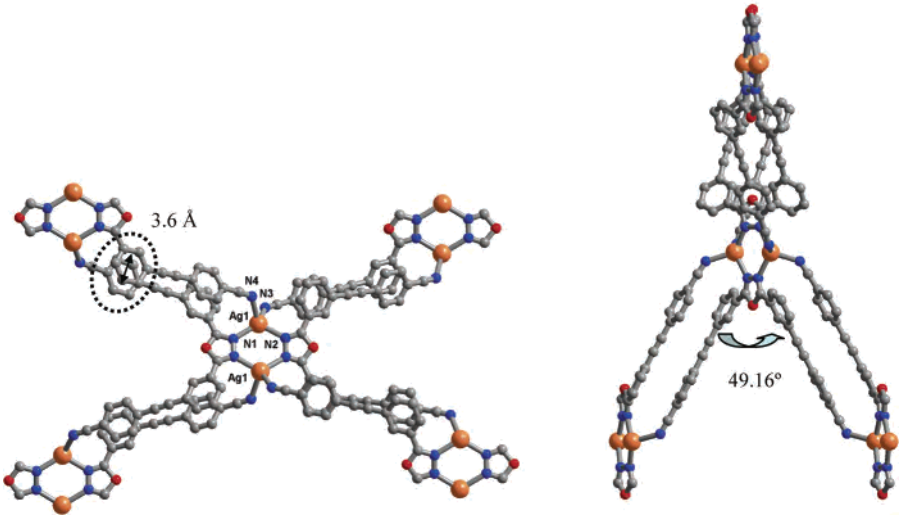

Figure 23. Doubly linked four-connected $\{Ag_2N_4\}$ cluster core building block in **7**.

using the PLATON program suggests that the effective volume for inclusion is 5948.6 Å^3, comprising 35.4% of the crystal volume (16 574.0 Å^3). It is noteworthy that the angle (49.16°) between two adjacent arms attached to the $\{Ag_2N_4\}$ cluster is smaller than that of **6**; The Ag···Ag separation in the $\{Ag_2N_4\}$ cluster core is 3.7 Å, which is longer than that of **6** by 0.2 Å. These tiny differences, however, play a central role in causing the changes of the crystal packing of **7** in the solid state. When viewed down the crystallographic *c* axis, in contrast to the regular honeycomb structure of **6**, the shape of the channels is twisted to a certain extent. When viewed down the crystallographic [10$\bar{1}$] direction, the coordination pattern is comparable to the [110] view of **6**, but with enclosed cylinderlike channels (Figure 25). There is no doubt that such a change results from the anion-templating effect (from BF_4^- to SbF_6^-). Counterion-dependent polymeric architectures have been observed quite often. However, the relationship between a given anion and the selective self-assembly of a certain type of polymeric motifs is not yet well-understood.

[Ag(L11)]ClO$_4$·(C$_7$H$_8$) (8). Complex **8** was prepared by reaction of $AgClO_4$ with the **L11** ligand in the required ratio in a THF/toluene mixed-solvent system. **8** crystallizes in the monoclinic space group *C*2/*c*, which is different from that of **6** and **7**, but it exhibits a 3-fold three-dimensional network in the solid state similar to that in **6** and **7**. As shown in Figure 26, the connecting node in **8** is a $\{Ag_2N_4O_2\}$ cluster core instead of the $\{Ag_2N_4\}$ moiety observed in **6** and **7**. The ClO_4^- anion acts as a $\mu-\eta^2$ ligand to bridge two crystallographically independent silver atoms on the Ag_2N_4 ring into a $\{Ag_2N_2O_2\}$ cluster core. The Ag···Ag separation within the disilver unit is ca. 3.5 Å, equivalent that of **6**. The angle (57.94°) between the two ethynylbenzonitrile-phenyl arms is smaller than that of **6** but larger than that of

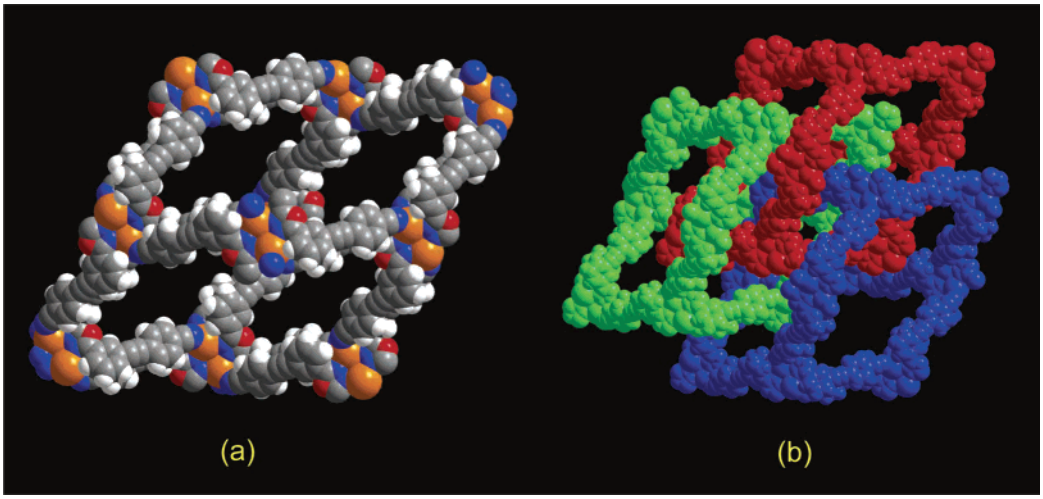

Figure 24. Space-filling diagram of the adamantoid cage formed in an individual framework (left), and an illustration of how the frameworks in **7** interpenetrate. The three independent frameworks are colored red, green, and blue (right).

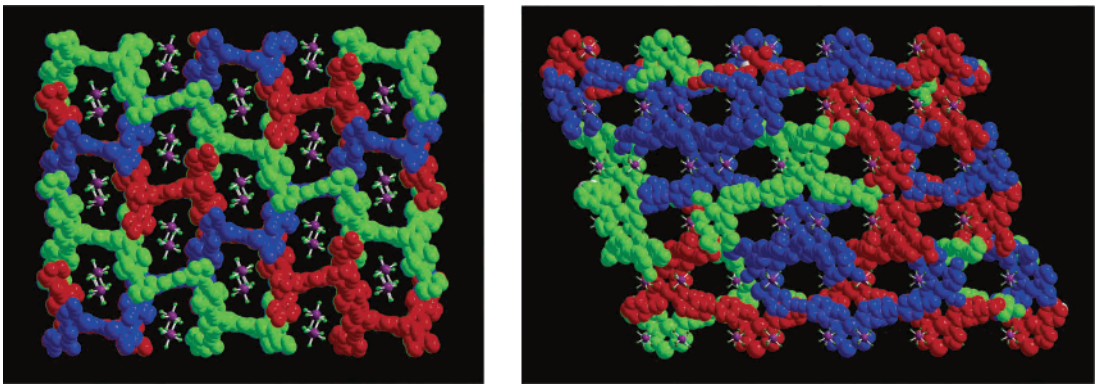

Figure 25. Three-fold interpenetration showing the twisted hexagonal (viewed down the *c* axis, left) and cylinder (viewed down [10$\bar{1}$] direction, right) channels. Frameworks are shown as space-filling models.

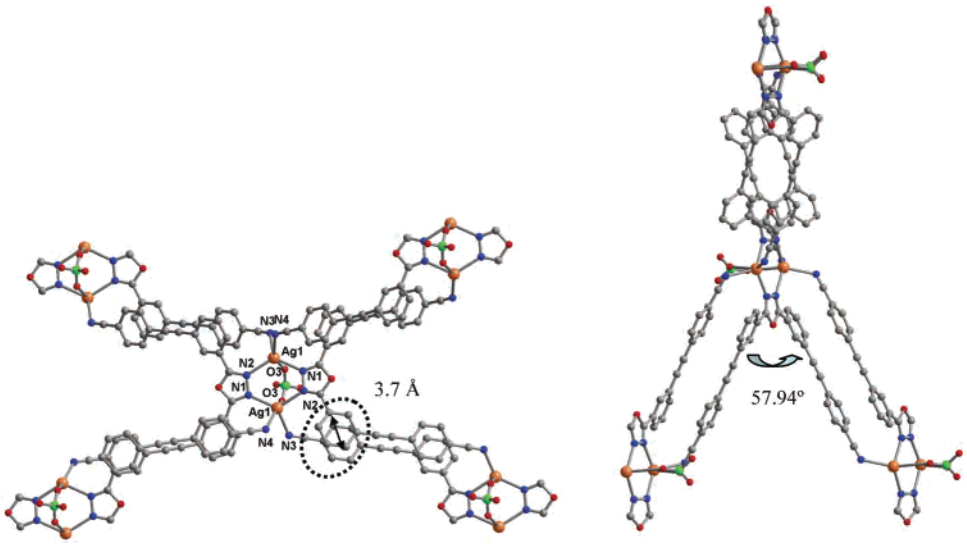

Figure 26. Doubly linked four-connected $\{Ag_2N_4\}$ cluster core building block in **8**.

7. Again, the interligand $\pi-\pi$ interactions present in **8** are due to the parallel arrangement of the ethynylbenzonitrile-phenyl linkages. By contrast with that of **6**, the 3-fold three-dimensional framework of **8** contains honeycomblike and elliptical channels with almost identical dimensions extending along the crystallographic *a* and [110] directions. ClO_4^- anions and toluene molecules are located in the cavities as guests (Figure 27). The solvent-accessible volume of 3470.6 Å^3 comprises 44.3% of the crystal volume (7826.0 Å^3). The $AgClO_4-$**L11** self-assembled structures (**5** and **8**) are not affected by the change in molar ratios (the 1:1 adduct was always isolated under different metal-to-ligand ratios);

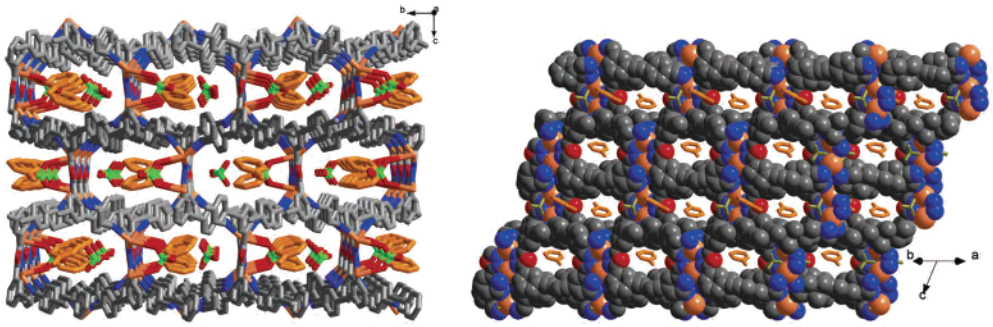

Figure 27. Three-fold interpenetration showing the regular hexagonal (viewed down the *a* axis, left) and elliptical channels. (viewed down the [110] direction, right).

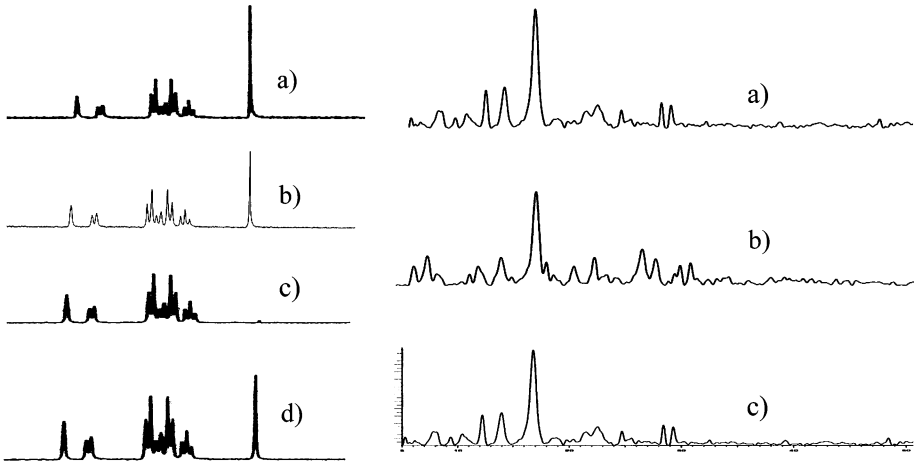

Figure 28. ^{1}H NMR spectra of **6** in DMSO-d^6 (left): (a) ^{1}H NMR spectrum of the original sample of **6** recorded at room temperature; (b) solid sample of **6** was heated to 110 °C and then dissolved in DMSO-d^6, the spectrum was recorded at ambient temperature; (c) solid sample of **6** was heated to 200 °C and then dissolved in DMSO-d^6, the spectrum was recorded at ambient temperature; (d) **6** immersed in benzene for 24 h and dried at room temperature for 1 day. X-ray powder diffraction patterns of **6** (right): (a) the original crystals of **6**; (b) **6** heated to 200 °C; (c) sample obtained by immersing (b) in benzene for 24 h at room temperature and dried at room temperature for 1 day.

however, they are strongly dependent upon the solvent templating. In other words, the solvent template readily gives rise to the change in conformations taken by **L11** during self-assembly. As mentioned above, compound **5** was isolated as a two-dimensional net from a CH_2Cl_2/benzene solvent system on the basis of conformation I, whereas **8** was separated as a three-dimensional framework from a THF/toluene solvent system generated from an intermediate conformation between conformation I and III. Thus, compounds **5** and **8** are solvent-responsive compounds because of the rotational freedom nature of **L11**.

As mentioned above, in all three three-dimensional structures **6**−**8**, the two long substituting arms attached to the central oxadiazole moiety are not coplanar and make the secondary building blocks three-dimensional, which causes the overall number of dimensions to go from two in **3**−**5** to three in **6**−**8**. The dihedral angles between the two ethynylbenzonitrilephenyl arms of **L11** in **6**−**8** are slightly different, which is reflected in the tiny different channel shapes observed in these three complexes.

Host−Guest Chemistry of Compound 6. Crystal engineering of organic−inorganic coordination network architectures on the basis of transition metals and organic spacers has attracted intensive attention. One of the most important motivations lies in that programmable crystal engineering may provide a new approach to the synthesis of functional nanoporous materials.[28] As a porous material, the important feature of **6** is that it can reversibly desorb and reabsorb benzene molecules (Figure 28).[29] TGA traces together with ^{1}H NMR spectra indicated that all benzene guest molecules could be removed at ∼200 °C. The framework of compound **6** is stable up to 220 °C. The X-ray powder diffraction pattern of thermally desolvated sample of **6** is compared with that of as-synthesized, solvent-containing **6**. The XRD pattern after heating shows that the shapes and intensities of some reflections are slightly changed relative to that of the original sample. This means that guest loss does not result in symmetry change or cavity volume collapse. When the desolvated solids are immersed in benzene for 24 h at room temperature, an XRD pattern nearly identical to that obtained for the original crystals is regenerated, indicating the benzene molecules were re-incorporated into the framework under these mild conditions. After the sample was taken out of

(28) (a) Bradshaw, D.; Claridge, J. B.; Cussen, E. J.; Prior, T. J.; Rosseinsky, M. J. **2005**, *38*, 273. (b) Ferey, G.; Mellot-Draznieks, C.; Serre, C.; Millange, F. *Acc. Chem. Res.* **2005**, *38*, 217.

(29) (a) Kondo, M.; Yoshiitomi, T.; Seki, K.; Matsuzaka, H.; Kitagawa, S. *Angew. Chem., Int. Ed.* **1997**, *36*, 1725. (b) Li, H.; Eddaoudi, M.; Groy, T. L.; Yaghi, O. M. *J. Am. Chem. Soc.* **1998**, *120*, 8571. (c) Li, H.; Eddaoudi, M.; O'Keeffe, M.; Yaghi, O. M. *Nature* **1999**, *402*, 276. (d) Choi, H. J.; Lee, T. S.; Suh, M. P. *Angew. Chem., Int. Ed.* **1999**, *38*, 1405. (e) Dybtsev, D. N.; Chun, H.; Yoon, S. H.; Kim, D.; Kim, K. *J. Am. Chem. Soc.* **2004**, *126*, 32. (f) Liao, Y.-C.; Liao, F.-L.; Chang, W.-K.; Wang, S.-L. *J. Am. Chem. Soc.* **2004**, *126*, 1320.

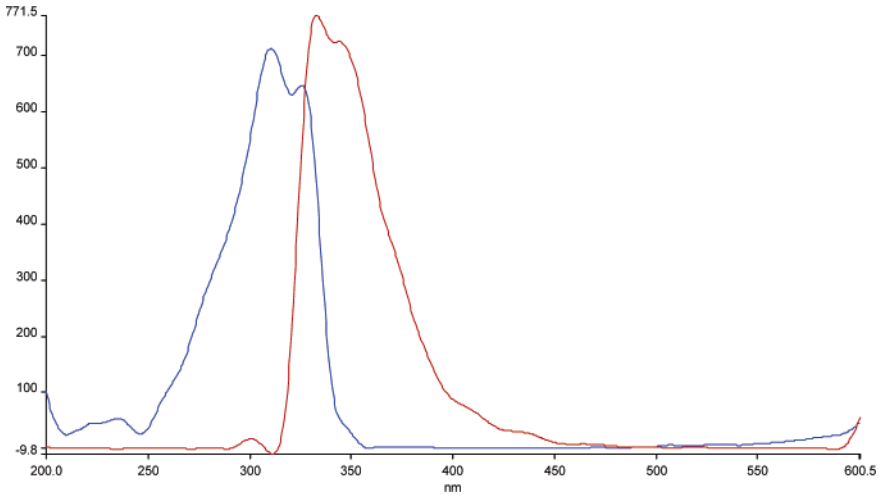

Figure 29. Photoinduced excitation (blue, 310 nm) and emission (red, 333 nm) spectra of **L11** in $CHCl_3$.

benzene, it was dried at room temperature for 24 h before the ^{1}H NMR spectrum was recorded. The ^{1}H NMR spectrum confirmed the re-uptake of benzene to the extent of 73%. Because **6** is insoluble in benzene, the possibility of a dissolution−recrystallization mechanism for explaining the solvent reabsorption is unlikely.

Luminescence Properties of L11 and Its Ag(I) Complexes. Inorganic−organic hybrid coordination polymers have been investigated for fluorescence properties and for potential applications as luminescence materials, such as light-emitting diodes (LEDs).[30] Because of the higher thermal stability of inorganic−organic coordination polymers and the ability to affect the emission wavelength of organic materials, syntheses of inorganic−organic coordination polymers by the judicious choice of conjugated organic spacers and transition-metal centers can be an efficient method for obtaining new types of electroluminescence materials, especially for d^{10} or d^{10}−d^{10} systems[31] and oxadiazole-containing complexes.[32] We have been exploring the luminescence properties of L1−L10 and organic−inorganic coordination polymers and supramolecular complexes based on these complexes in the solid state. The results indicate that emission colors of organic spacers L1−L10 were affected by their incorporation into metal-containing coordination compounds.[14] The luminescence properties of **L11** and polymeric compounds **1**−**3**, **5**, **6**, and **8** were investigated in the solid state. The fluorescence spectra of **L11** and its complexes are summarized in Table 11. As indicated in Figure 29, in $CHCl_3$, **L11** presents one maximum at 333 nm, with a second, less-intense band present at 345 nm. In the solid state, **L11** exhibits one emission maximum at 380 nm. As shown in Table 11, in the solid state, the emission color of the free ligand was significantly affected by its incorporation into the Ag-containing polymeric complexes, as evidenced by the large red shift (33−43 nm) in the emission. Reasonably, the presence of the intervening silver atoms, which exert an electron-withdrawing effect as a consequence of their +1 charge, have a significant influence on the luminescence properties of the ligand. In CH_3CN, the emission colors between **L11** and its silver complexes are almost identical, which implies that the polymeric complexes disaggregate into starting materials in acetonitrile.

Table 11. Luminescence Properties of **L11** and Complexes **1**−**3**, **5**−**6**, and **8** in the Solid State

compd	solid state ($\lambda_{ex}/\lambda_{em}$)	compd	solid state ($\lambda_{ex}/\lambda_{em}$)
L11	358/380	**5**	360/414
1	376/413	**6**	355/423
2	386/422	**8**	369/421
3	365/423		

Conclusions

In conclusion, one nanosized oxadiazole bridging ligand, **L11**, was designed and synthesized by the reaction of bis-(3-iodophenyl)oxadiazole with 4-cyanophenylacetylene via a classical Sonogashira−Hagihara cross-coupling reaction. Eight Ag(I)−**L11** coordination polymers with one-, two- and three-dimensional structures have been successfully prepared by the reaction of **L11** with various Ag(I) salts in solution. All new complexes are capped by a silver cluster core ($\{Ag_2O_2N_2\}$ in **1** and **2**, $\{Ag_2N_4\}$ in **3**−**7**, and $\{Ag_2N_2O_2\}$ in **8**) instead of a simple metal ion, and the **L11** doubles up in the frameworks. A cluster node and double rungs participated in the $\pi-\pi$ interaction, making the secondary building block bulk up, which appears to inhibit high interpenetration; this effectively facilitates the formation of large channels or cavities in aggregates. In this Ag(I)−**L11**

(30) (a) Ciurtin, D. M.; Pschirer, N. G.; Smith, M. D.; Bunz, U. H. F.; zur Loye, H.-C. *Chem. Mater.* **2001**, *13*, 2743. (b) Cariati, E.; Bu, X.; Ford, P. C.; *Chem. Mater.* **2000**, *12*, 3385. (c) Würthner, F.; Sautter, A. *Chem. Commun.* **2000**, 445.
(31) (a) Harvey, P. D.; Gray, H. B. *J. Am. Chem. Soc.* **1988**, *110*, 2145. (b) Catalano, V. J.; Kar, H. M.; Bennett, B. L. *Inorg. Chem.* **2000**, *39*, 121. (c) Tong, M.-L.; Chen, X.-M.; Ye, B.-H.; Ji, L.-N. *Angew. Chem., Int. Ed.* **1999**, *38*, 2237. (d) Burini, A.; Bravi, R.; Fackler, J. P., Jr.; Galassi, R.; Grant, T. A.; Omary, M. A.; Pietroni, B. R.; Staples, R. J. *Inorg. Chem.* **2000**, *39*, 3158. (e) Seward, C.; Jia, W.-L.; Wang, R.-Y.; Enright, G. D.; Wang, S.-N. *Angew. Chem., Int. Ed.* **2004**, *43*, 2933. (f) Yam, V. W.-W.; Lo, K. K.-W. *Chem. Soc. Rev.* **1999**, *28*, 323. (g) Wu, C.-D.; Ngo, H. L.; Lin, W. *Chem. Commun.* **2004**, 1588.
(32) (a) Hu, N.-X.; Esteghamatian, M.; Xie, S.; Popovic, Z.; Hor, A.-M.; Ong, B.; Wang, S.-N. *Adv. Mater.* **1999**, *11*, 1460. (b) de Silva, A. S.; de Silva, M. A. A.; Carvalho, C. E. M.; Antunes, O. A. C.; Herrera, J. O. M.; Brinn, I. M.; Mangrich, A. S. *Inorg. Chim. Acta* **1999**, *292*, 1. (c) Wang, J.; Wang, R.; Yang, J.; Zheng, Z.; Carducci, M. D.; Cayou, T.; Peyghambarian, N.; Jabbour, G. E. *J. Am. Chem. Soc.* **2001**, *123*, 6179.

system, the conformation of **L11** is versatile and depends greatly on the counterion and solvent system used in the formation of the complexes: (a) in one-dimensional structures **1** and **2**, the ligand displays conformation II with the central oxadiazole and its two adjacent phenyl rings being coplanar; (b) in two-dimensional compounds **3**−**5**, **L11** takes either conformation I or II but with the central oxadiazole and two neighbor phenyl rings being nonplanar; and (c) in three-dimensional compounds **6**−**8**, **L11** chooses an intermediate conformation between I and III, with the two long cyanophenylacetylene arms lying in different planes. Clearly, we still have a lot to learn about how exactly to control the conformation of **L11** taken during the self-assembly process. Nevertheless, the self-assembly of the bent organic ligands with long rigid sidearms connected by a central coordinated heterocyclic ring and metal ions is a new approach for accessing metal−organic frameworks consisting of double rungs and metal cluster nodes. We are currently extending this result by preparing new symmetric and unsymmetric five-membered heterocyclic ring bridging ligands of this type that contain different coordination functional groups and have different orientations of the terminal coordination sites. The new metal−organic polymers and supramolecular complexes based on the new bent spacers of this type with novel polymeric patterns and properties will be reported soon.

Acknowledgment. We are grateful for financial support from the National Natural Science Foundation of China (No. 20371030), and Shangdong Natural Science Foundation (No. Z2004B01).

Supporting Information Available: Crystallographic data in cif format. This material is available free of charge via the Internet at http://pubs.acs.org.

IC052158W